DØ note 6143 [Version 1.4]

Correction For the MC-Data Difference in the Jet Response at DØ

S. Atkins, K. Augsten, S. Evstyukhin, A. Juste, M. Wang, Z. Ye

February 7, 2011

Abstract

Jet responses are different between Monte Carlo (MC) simulation and data for the DØ experiment. Such a difference not only changes with the jet kinematics, but also with the flavor of the partons which initiate the jets. In this note, we describe a method to correct the MC simulation so that it has the same kinematic and flavor-dependent jet response as that in data. We present the results for DØ Run IIA MC and data JCCB jets.

Contents

1 Introduction

In a hadron collider, jets are produced from the fragmentation of quarks and gluons generated in hard scattering processes. At DØ, the jets are reconstructed by the so-called "Run II Midpoint Cone Algorithm" with a cone size of $R = 0.5$ (JCCB) or $R = 0.7$ (JCCA). This algorithm can be applied both at the stable particle (particle jets) and the reconstructed calorimeter tower (calorimeter jets) levels. The raw energy of a calorimeter jet is estimated to be the sum of energies over all towers included in the jet. It is then corrected on average to the particle level by the jet energy scale (JES) for physics, instrumental and jet algorithm-dependent effects.

The JES depends on the jet kinematics, e.g., transverse momentum p_T and detector pseudo-rapidity η_{det}. It also depends on the topological configuration of the jet, e.g., type, energy and angular spectra of particles constituting the jet. Jets initiated from different flavors of parent partons have different topologies (see Fig. 1), and jets produced in different processes have different parent parton flavor compositions. This lead to a sample-dependent (or rather flavor-dependent) JES.

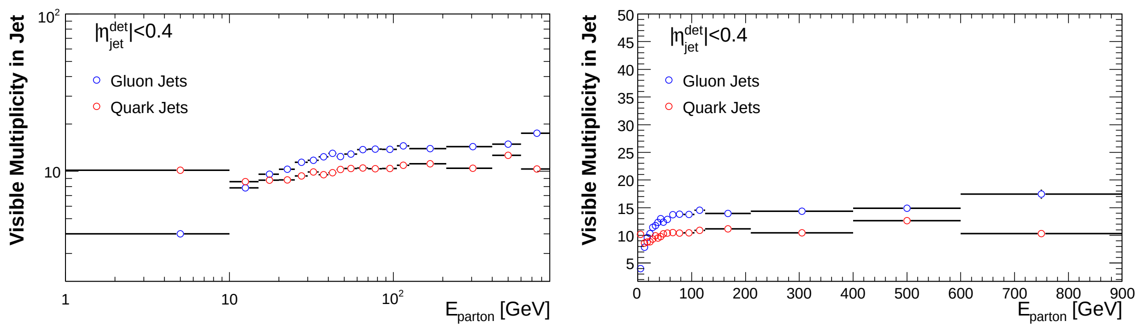

Figure 1: Number of particles (excluding neutrinos) in particle jets produced by quarks or gluons in Pythia γ+jet MC samples. Left: in log-scale, Right: in linear-scale. The x-axis is the energy of quarks or gluons, and the y-axis the number of particles (excluding neutrinos) in particle jets.

The standard JES correction at DØ is derived, separately for the MC simulation and data, from samples enriched in γ+jet or di-jets events. It takes into account the kinematic dependence of the JES, but not the flavor dependence. For analyses which calibrate the data analysis results using the MC simulation, the flavor dependence is not so important if the MC simulation does a good job in describing the data. It is the case at CDF which tunes their detector simulation so that it has the same single (charged) pion response as that measured from the collider and test beam data [1]. It is not the case at DØ which has different single (charged) pion responses between the MC simulation and data [2].

This sample-dependent MC-data difference in the jet response has been accounted for as systematic uncertainties in top quark measurements at DØ, including

(a) difference in the b and light jet response ratio between the MC and data;

(b) difference in the quark and gluon jet response ratio between the MC and data.

For the DØ top quark mass measurement using the matrix element method in the lepton+jets channel, the contribution to the systematic uncertainty from (a) was estimated to be about 0.8 GeV [3], based on the MC and data charged pion responses extracted in a Run IIA JES study for high energy extrapolation of the jet response of the data [2]. Using these MC and data charged pion responses, it was estimated that the ratio between the b and light jet response in the MC was higher by about 1.8% than that in data [4]. The systematic uncertainty associated with (a) was then given by the difference between the top quark mass measured from the default MC and that from a modified MC in which the JES-corrected b jet energy and momentum was scaled down by 1.8%. The systematic uncertainty due to (b) was estimated to be about 0.6 GeV [3], given by the difference between the top quark mass measured from the MC with JSSR shifting turned on and that with shifting turned off. While this is a very rough estimation that is not believed to reflect the truth, it has been the only officially accepted way used to estimate this systematic uncertainty. The above two together contribute 1.0 GeV to the systematic uncertainty of the DØ top quark mass measurement using the matrix element method in the lepton+jets channel. (Note the corresponding number at CDF is 0.2 GeV.)

This note describes a method to correct the MC for the MC-data difference in the jet response. Results on JCCB jets for Run IIA MC and data are presented. Results on JCCA jets and results for the Run IIB

MC and data will be presented in separate notes. The note is organized as the following. Section 2 gives a brief description of the method. Section 3 describes the extraction of MC single particle responses and the closure test for the extracted MC responses. Section 4 describes the extraction of data single particle responses and the closure test for the extracted data responses. Section 5 presents the MC-data correction factor averaged for different flavor of jets. Section 6 presents an estimation for the uncertainty of the MC-data correction factor. Section 5.1 presents a brief discussion on the influence of this corretion on the JSSR (Shifting, Smearing and Removing Simulated Jets).

2 The Correction Method

For each calorimeter jet in the MC, we look for a spatially matched particle jet to calculate the correction factor F

$$F = \frac{\sum_i E_i \cdot R_i^{data}}{\sum_i E_i \cdot R_i^{MC}}, \tag{1}$$

where the subscript i runs over the particles in the particle jet, E_i are the energies of the particles and R_i the single particle responses in MC or data. This correction factor corrects for the MC-data difference in the jet response and should be applied to the jet energy after the offset correction [2], i.e.,

$$(E_{jet}^{raw} - E_O) \cdot F = (E_{jet}^{raw} - E_O) \cdot \frac{\sum_i E_i \cdot R_i^{data}}{\sum_i E_i \cdot R_i^{MC}}, \tag{2}$$

where E_{jet}^{raw} is the raw jet energy, E_O the offset correction for noise, pile-up and multiple interactions. The other JES corrections (response, showering, etc) should be applied on $(E_{jet}^{raw} - E_O) \cdot F$ as usual [2].

Note that Eq. 1 assumes that observed energies are well-approximated by a linear combination of the energies of the individual particles. We will describe how deviations from this approximation show up in the MC closure test in section 3 and quantify the resulting systematic uncertainties in section 6.1.

The ingredients needed for F include the matched particle jet with associated particles, the single particle responses in MC and data. The extraction of MC and data single particle responses are described in section 3 and 4. Particle jets are reconstructed with a cone size of $R = 0.5$ in the Run II E-scheme using pxcone package. Except the neutrinos, all the other *stable* particles γ, $e^{\pm}$, $\mu^{\pm}$, $\pi^{\pm}$, $K^{\pm}$, K_0^S, K_0^L, $p^{\pm}$, n, Λ, Σ's and Ξ's are included to reconstruct the particle jet. Note that most of the energy in the particle jets are coming from $\pi^{\pm}$ and γ. The matching between the particle jet and calorimeter jet is based on the angular separation $\Delta R = \sqrt{\Delta\phi^2 + \Delta\eta^2}$ between the two. We regard the particle jet that has the smallest ΔR to the calorimeter jet as the one which makes the calorimeter jet. The maximum allowed value of ΔR to claim a particle jet being matched to a calorimeter jet is 0.25 for JCCB jets.

The method developed in this study to extract the data single particle responses follows partially the Run IIA JES study done for high energy extrapolation of the jet response of the data [2]. In the Run IIA JES study, reconstruction was re-run each time with the energy deposition by charged pions in the calorimeter in the MC being varied. By doing this, the MC charged pion response was tuned so that the MC had the same jet response as that in data. The differences of the approach presented here to the one in the Run IIA JES study include:

- We use the spatially matched particle jets and MC and data single particle responses, and calculate the MC-data correction factor on-the-fly, while the Run IIA JES study varied directly the energy deposition of the charged pions in the calorimeter and re-run the reconstruction;
- We consider the difference in the calorimeter response between the MC and data for all the particles, while the Run IIA JES study only considered that for the charged pions;
- We study jets with $|\eta_{det}| < 2.5$, taking into account the variation of the calorimeter response versus η_{det}, while the Run IIA JES study only considered jets with $|\eta_{det}| < 0.4$ assuming a flat η_{det}-dependence of the charged pion response.

Previous studies for the difference in the b and light jet response ratio between the MC and data [4] and sample-dependent JES [5] also calculated the correction factor for the MC-data difference in the jet response, using the MC and data single pion responses from the Run IIA JES study as inputs. The differences of the approach presented here to the previous ones include:

- We extract the MC single particle responses for γ, $e^{\pm}$, $\mu^{\pm}$, $\pi^{\pm}$, $K^{\pm}$, K_0^S, K_0^L, $p^{\pm}$, n and Λ from single particle MC samples in different η_{det} region, while the previous studies used the MC single responses for γ, $e^{\pm}$, $\pi^{\pm}$, $K^{\pm}$ and $p^{\pm}$ from the Run IIA JES and W-mass analyses which were performed only in the central calorimeter region. It was assumed that the responses did not change with η_{det}. As shown in section 3, such an assumption is far away from the truth;

- We extract the data single particle responses in different calorimeter region, while the previous studies used the data single particle responses extracted in the Run IIA JES study that was performed only for $|\eta_{det}| < 0.4$.

3 Extracting MC Single Particle Responses

The MC single particle responses are measured for γ, $e^{\pm}$, $\mu^{\pm}$, $\pi^{\pm}$, $K^{\pm}$, K_0^S, K_0^L, $p^{\pm}$, n and Λ from Run IIA single particle MC samples, with all the zero suppression (ZS)[1], calorimeter noise and zero bias (ZB) overlay turned off. For each single particle, the energy of the calorimeter cells contained in the $R = 0.5$ cone around the particle are summed over to give the MC single particle response, defined as the measured energy divided by the MC truth energy. The results are shown in Fig. 22-31. The parameterizations of the fitting functions, which are found to best describe the MC responses with the minimul number of parameters, are:

$$R_\gamma^{MC} = 0.25 \cdot p_\gamma^0 \cdot \left[1 + Erf\left(\frac{E + p_\gamma^1}{\sqrt{2 \cdot p_\gamma^2}}\right)\right]\left[1 + Erf\left(\frac{E + p_\gamma^3}{\sqrt{2 \cdot p_\gamma^4}}\right)\right] + p^5, \quad (3)$$

$$R_{e^\pm}^{MC} = 0.25 \cdot p_{e^\pm}^0 \cdot \left[1 + Erf\left(\frac{E + p_{e^\pm}^1}{\sqrt{2 \cdot p_{e^\pm}^2}}\right)\right]\left[1 + Erf\left(\frac{E + p_{e^\pm}^3}{\sqrt{2 \cdot p_{e^\pm}^4}}\right)\right] \text{ if } p_T > 0.3;\ 0 \text{ if } p_T < 0.3, \quad (4)$$

$$R_{\mu^\pm}^{MC} = (p_{\mu^\pm}^0 + p_{\mu^\pm}^1 \cdot E) \cdot \text{TMath :: Landau}(E, p_{\mu^\pm}^2, p_{\mu^\pm}^3) \text{ if } p_T > 0.3;\ 0 \text{ if } p_T < 0.3, \quad (5)$$

$$R_h^{MC} = p_h^0 \cdot \left[1 - p_h^1 \cdot (E/0.75)^{p_h^2 - 1}\right] \text{ if } p_T > 0.3;\ 0 \text{ if } p_T < 0.3, \quad (6)$$

$$(7)$$

where $h = \pi$, $K^{\pm}$, K_0^S, K_0^L, $p^{\pm}$, n or Λ. The fitted results can be found in Fig. 22-31.

As can be seen, the MC single particle responses from the Run IIA JES and W-mass studies only agree to some extent with the ones of this study. As also can be seen, the MC single particle responses change versus η_{det} and thus the assumption made in the previous studies [4, 5] that one can apply the MC and data single particle responses in the central calorimeter region to the entire calorimeter is invalid.

We check how well the denominator in Eq. 2, $\sum_i E_i \cdot R_i^{MC}$, describes the MC raw jet energy after the offset correction $(E_{jet}^{raw} - E_O) \cdot k_O$, where k_O is the correction for the ZS bias for the offset correction. We refer to the above check as the MC closure test in the following. We use E_O and k_O measured for the standard JES correction. Note that k_O is needed to perform the MC closure test, but not for estimating F in Eq. 1.

The MC closure test results for jets in γ+jet MC samples are shown in Fig. 2-6. Reasonable agreements shown in these plots increase our confidence to use the particle jets to obtain the MC-data correction factor by Eq. 1. The goodness of the E_O and k_O used here can be verified by comparing the above results with the MC closure test results for γ+jet MC samples produced without ZB overlay. The offset corrections E_O or k_O is not applied to the latter, which are shown in Fig. 32-36. The fact that the two sets of results shown in Fig. 2-6 and in Fig. 32-36 agree with each other indicates that E_O and k_O used here correct properly for noise, pile-up and multiple interactions, which are simulated in the MC by the ZB overlay.

We also note that the ratio between $(E_{jet}^{raw} - E_O) \cdot k_O$ and $\sum_i E_i \cdot R_i^{MC}$ is not perfectly at one. We consider this residual of the closure test as a systematic uncertainty for the MC-data correction factor F, as described in section 6.1.

4 Extracting Data Single Particle Responses

The extraction of data single particle responses follow partially the Run IIA JES study for high energy extrapolation [2]. Briefly speaking, what was done in [2] and we are doing here is to tune the MC jet responses by tuning the underlying MC single particle responses so that the MC jet response agrees with

[1] Hereafter we refer zero suppression to both online readout and offline reconstruction thresholds as well as the T42 algorithm.

that in data, and one can use the corresponding tuned MC single particle responses as the data single particle responses.

We make the assumption that MC does a good job in simulating the EM component of the calorimeter, as well as the muon interaction within the detector. Therefore the MC has the same photon, electron and muon responses as those in data:

$$R_{\gamma}^{data} = R_{\gamma}^{MC}, \quad (8)$$

$$R_{e^{\pm}}^{data} = R_{e^{\pm}}^{MC}, \quad (9)$$

$$R_{\mu^{\pm}}^{data} = R_{\mu^{\pm}}^{MC}. \quad (10)$$

Note that the same assumption was made not only for photon, electron and muon but also for all the particles except the charged pions in the Run IIA JES study [2]. In section 6.2, we estimate the uncertainty on the correction factor F due to this assumption.

For the hadrons, we introduce three additional parameters A, B and C into Eq. 6 to parametrize the difference between MC and data:

$$R_h^{data} = C \cdot p_h^0 \cdot \left[1 - A \cdot p_h^1 \cdot (E/0.75)^{p_h^2+B-1}\right] \text{ if } p_T > 0.3;\ 0 \text{ if } p_T < 0.3, \quad (11)$$

where $R_h^{data} = R_h^{MC}$ when $A = C = 1$ and $B = 0$. Thus the correction factor F defined in Eq. 1 depends on A, B and C through Eq. 11.

The tuning of the MC jet responses is made by changing A, B and C in Eq. 11 which enters into Eq. 2. We select MC and data events with one CC photon and one jet back-to-back. The MC samples used here are Pythia γ+jet and di-jets events, which are combined according to their cross sections. The data sample used here is the Run IIA EMinclusive skim. Details of the object reconstruction and event selection can be found in [2]. For each selected event in MC and data, we calculate the ratio between the transverse momentum of

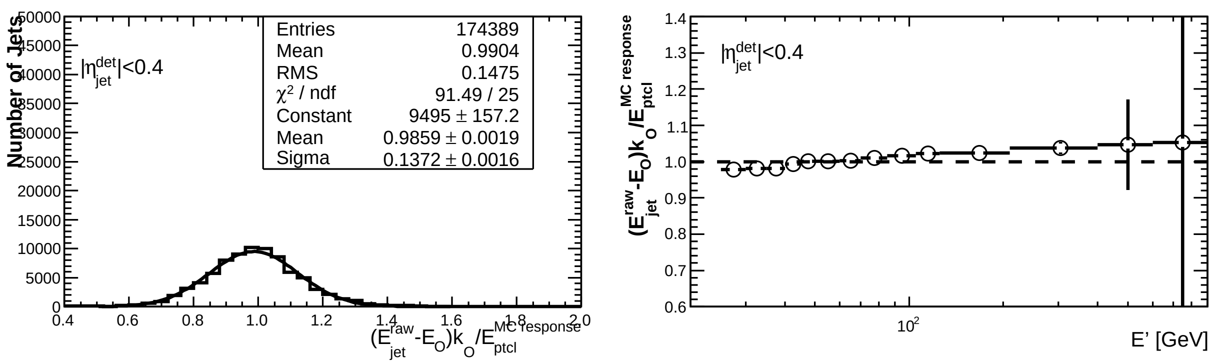

Figure 2: MC closure test for jets in p17 γ+jet MC sample for $|\eta_{det}^{jet}| < 0.4$. The single particle MC responses are derived with ZS turned off. The x-axis E' is given by $p_T^{\gamma} \cdot cosh(\eta^{jet})$.

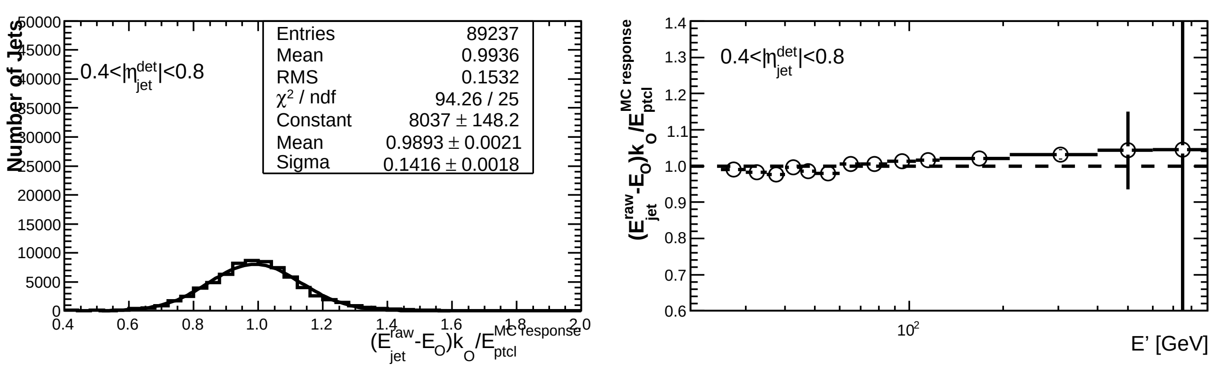

Figure 3: MC closure test for jets in p17 γ+jet MC sample for $0.4 < |\eta_{det}^{jet}| < 0.8$. The single particle MC responses are derived with ZS turned off. The x-axis E' is given by $p_T^{\gamma} \cdot cosh(\eta^{jet})$.

the photon p_T^γ and the transverse momentum of the jet $p_T^{jet,corrected}$ after the offset correction for data and after the offset correction and the correction in Eq. 1 for MC:

$$p_{T,\ corr}^{jet} = p_{T,\ raw}^{jet} \cdot \frac{E_{raw}^{jet} - E_O}{E_{raw}^{jet}} \cdot F(A, B, C) \text{ for MC,} \tag{12}$$

$$p_{T,\ corr}^{jet} = p_{T,\ raw}^{jet} \cdot \frac{E_{raw}^{jet} - E_O}{E_{raw}^{jet}} \text{ for data.} \tag{13}$$

We tune the parameters A, B and C so that the ratio $p_{T,\ corr}^{jet}/p_T^\gamma$ from MC is consistent to that from data.

The tuning of MC to data is done as the following. We fill a profile histogram of $p_{T,\ corr}^{jet}/p_T^\gamma$ versus

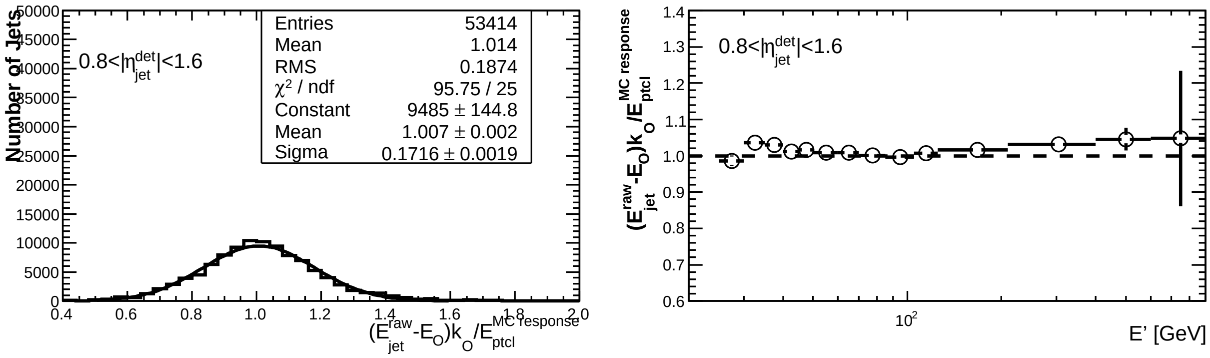

Figure 4: MC closure test for jets in p17 γ+jet MC sample for $0.8 < |\eta_{det}^{jet}| < 1.6$. The single particle MC responses are derived with ZS turned off. The x-axis E' is given by $p_T^\gamma \cdot cosh(\eta^{jet})$.

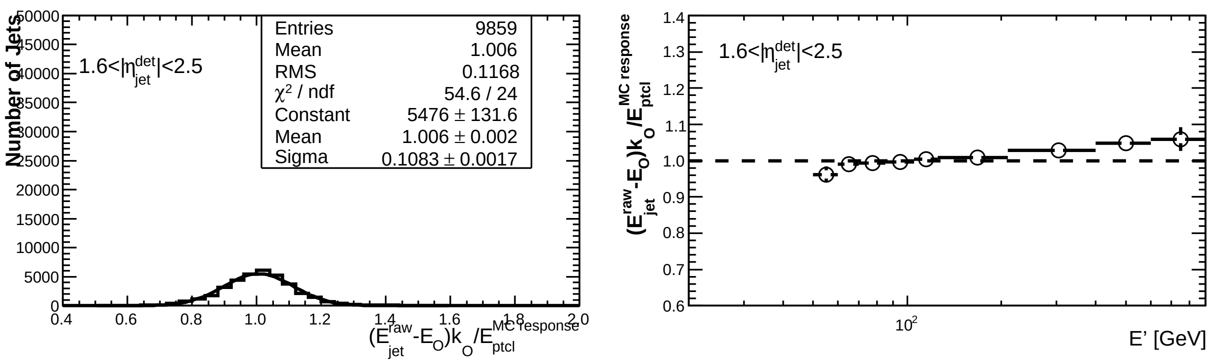

Figure 5: MC closure test for jets in p17 γ+jet MC sample for $1.6 < |\eta_{det}^{jet}| < 2.5$. The single particle MC responses are derived with ZS turned off. The x-axis E' is given by $p_T^\gamma \cdot cosh(\eta^{jet})$.

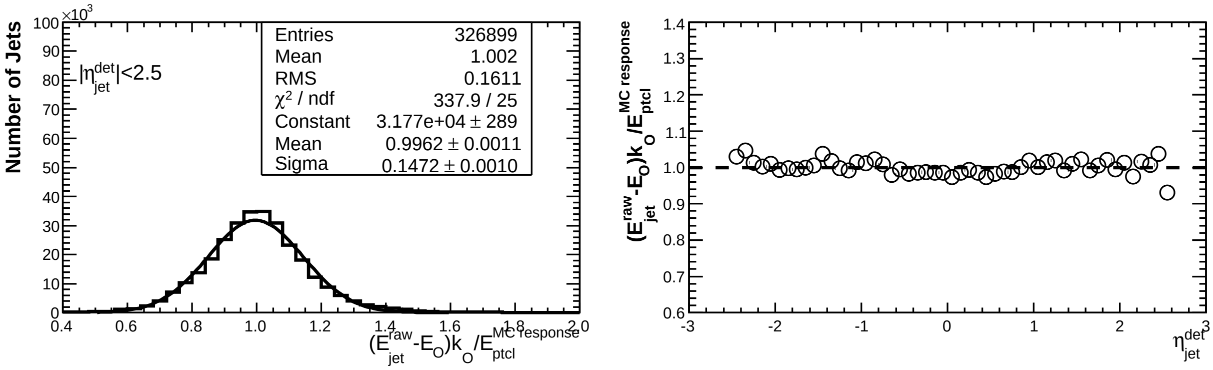

Figure 6: MC closure test for jets in p17 γ+jet MC sample for $|\eta_{det}^{jet}| < 2.5$. The single particle MC responses are derived with ZS turned off. The x-axis E' is given by $p_T^\gamma \cdot cosh(\eta^{jet})$.

$E' = p_T^{\gamma}/cosh(\eta^{jet})$ for data. For MC we scan over A, B and C. At each set of A, B and C values, we fill a profile histogram as above, then fit the histogram to a 3rd order polynomial function and calculate a χ^2 value using the fitted polynomial function and the data points. We look for the place where this χ^2 is the smallest. Note that this is the same approach as the Run IIA JES study.

The tuning is performed simultaneously for two different event selections: tight photon selection in which we apply tight photon isolation cuts to select γ+jet events, and apply the same photon selection cuts except a reversed track isolation requirement and select mainly di-jets events. The two selections have different compositions of quark and gluon jets, as shown in Fig. 7. The simultaneous tuning in the two event selections are shown in Fig. 8-9. The uncertainties on the parameters A, B and C are propagated to the MC-data correction factor F defined in Eq. 1, as described in section 6.3.

We perform a closure test for the above MC tuning procedure. The results are shown in Fig. 10-17. As can be seen, the jet responses from the corrected MC are consistent with those in data, for both tight photon and reversed photon selections which have different jet flavor composition.

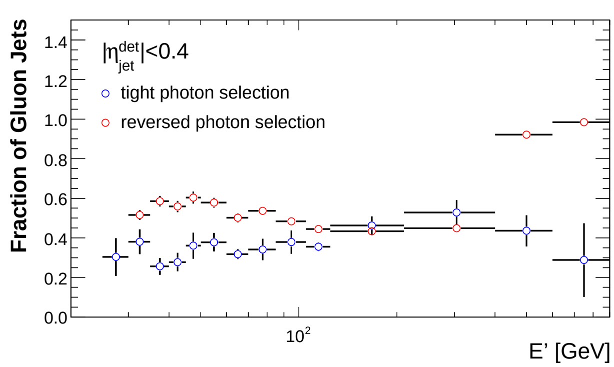

Figure 7: Fraction of gluon jets in the combined γ+jet and di-jets MC sample passed tight or reversed photon selection.

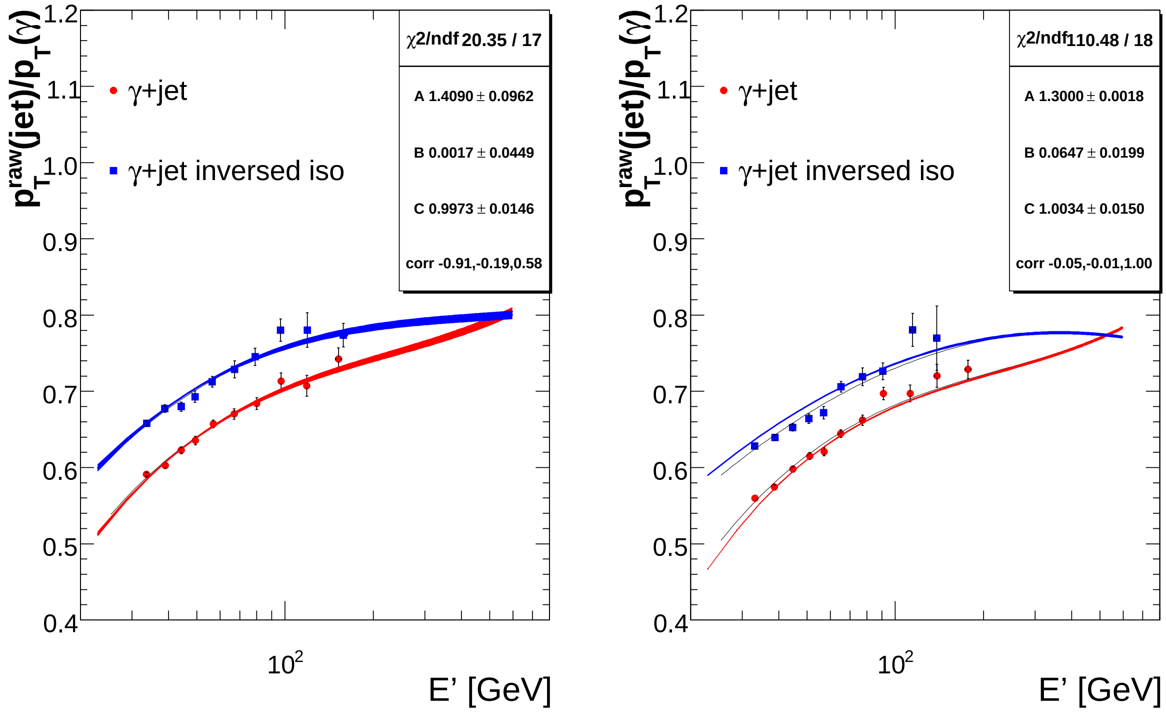

Figure 8: MC tuning for $|\eta_{det}^{jet}| < 0.4$ (left) and $0.4 < |\eta_{det}^{jet}| < 0.8$ (right). The points are data. The bands are MC tuning with the smallest χ^2 as described in the text.

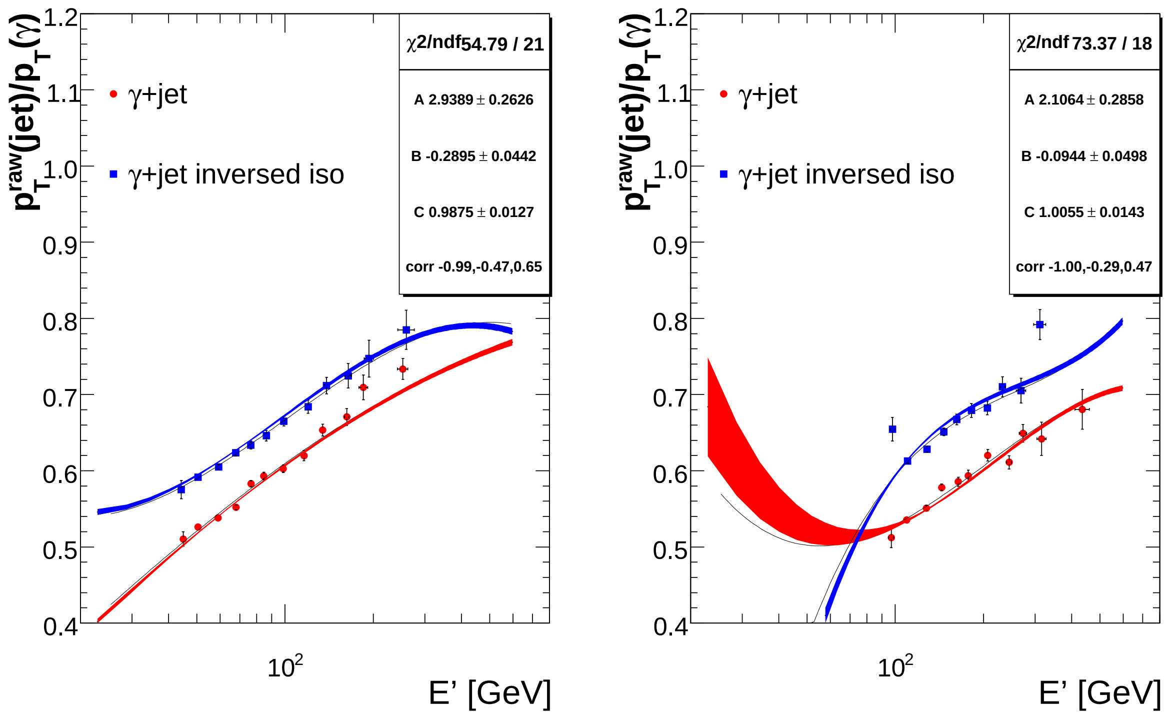

Figure 9: MC tuning for $0.8 < |\eta_{det}^{jet}| < 1.6$ (left) and $1.6 < |\eta_{det}^{jet}| < 2.5$ (right). The points are data. The bands are MC tuning with the smallest χ^2 as described in the text.

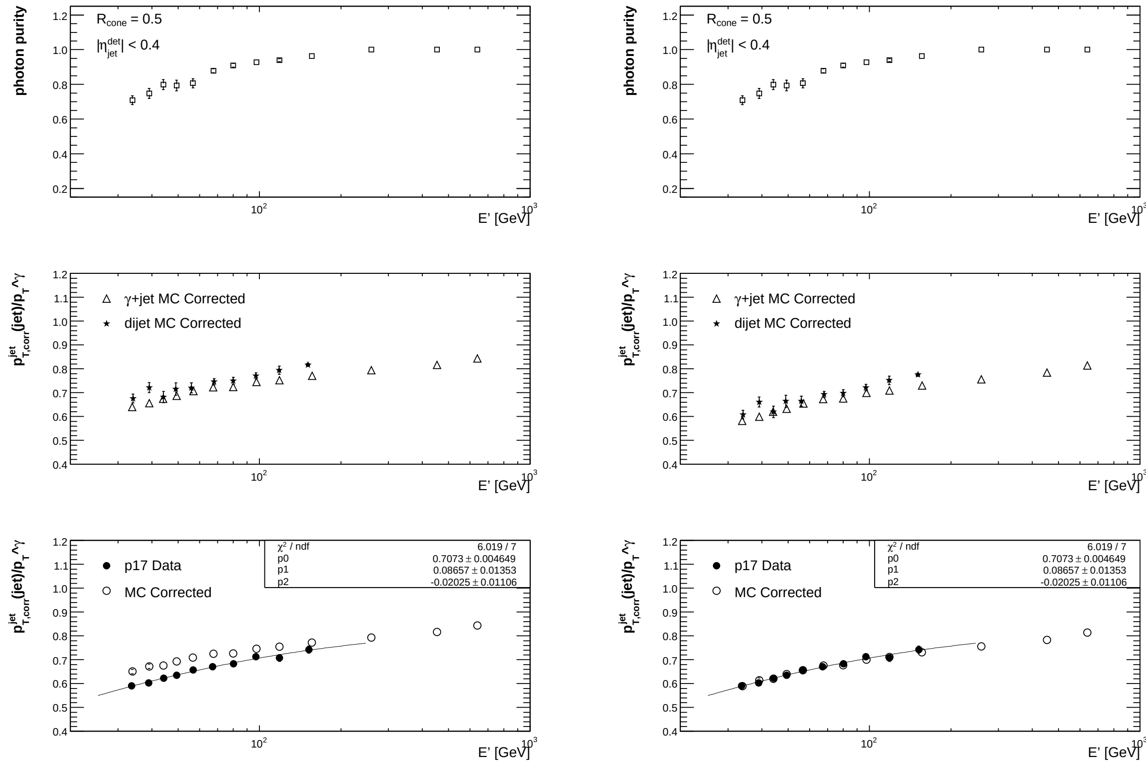

Figure 10: Closure test for MC tuning to data for tight photon selection with $|\eta_{det}^{jet}| < 0.4$. Photon purity (top), γ+jet and di-jets MC responses (middle) and combined γ+jet and di-jets MC response compared to data (bottom). Left: default MC; right: MC after tuning.

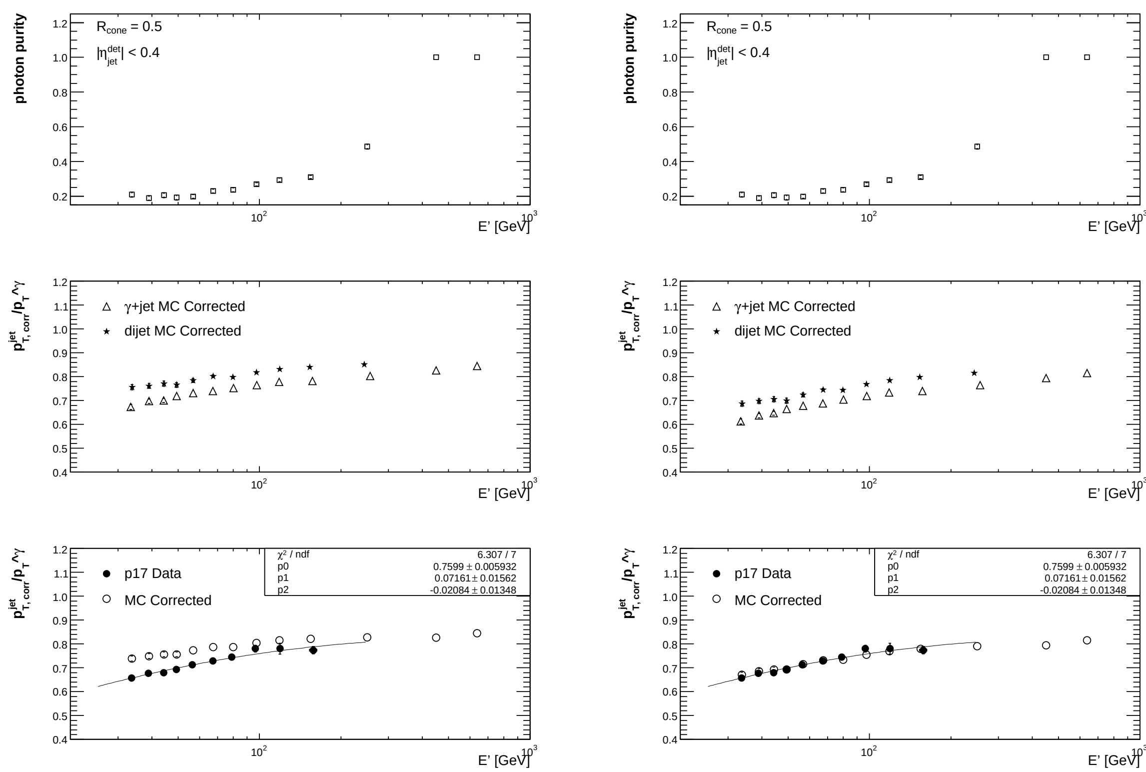

Figure 11: Closure test for MC tuning to data for reversed photon selection with $|\eta_{det}^{jet}| < 0.4$. Photon purity (top), γ+jet and di-jets MC responses (middle) and combined γ+jet and di-jets MC response compared to data (bottom). Left: default MC; right: MC after tuning.

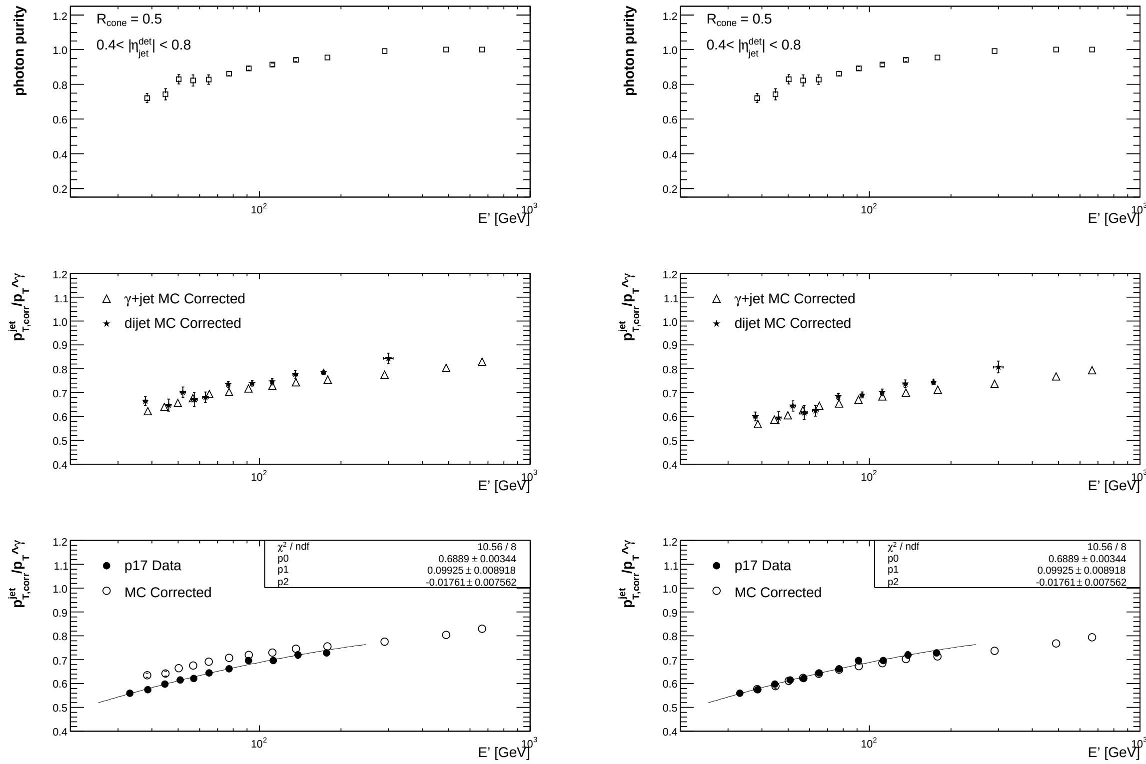

Figure 12: Closure test for MC tuning to data for tight photon selection with $0.4 < |\eta_{det}^{jet}| < 0.8$. Photon purity (top), γ+jet and di-jets MC responses (middle) and combined γ+jet and di-jets MC response compared to data (bottom). Left: default MC; right: MC after tuning.

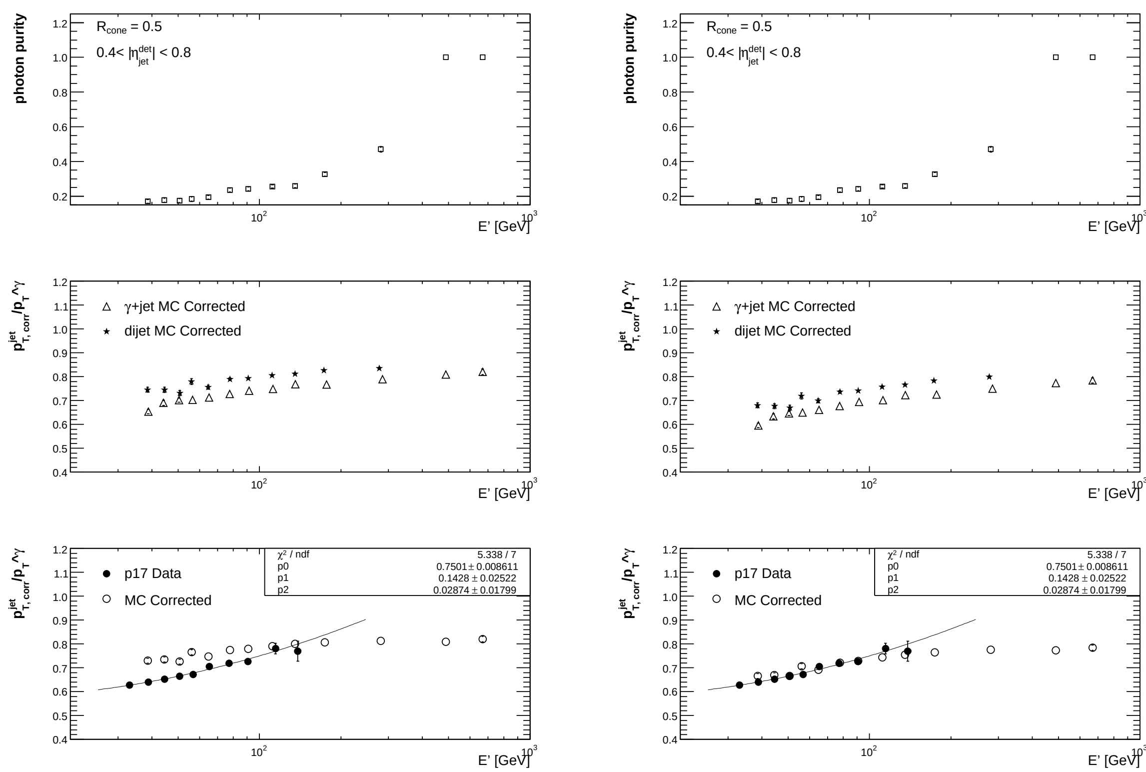

Figure 13: Closure test for MC tuning to data for reversed photon selection with $0.4 < |\eta_{det}^{jet}| < 0.8$. Photon purity (top), γ+jet and di-jets MC responses (middle) and combined γ+jet and di-jets MC response compared to data (bottom). Left: default MC; right: MC after tuning.

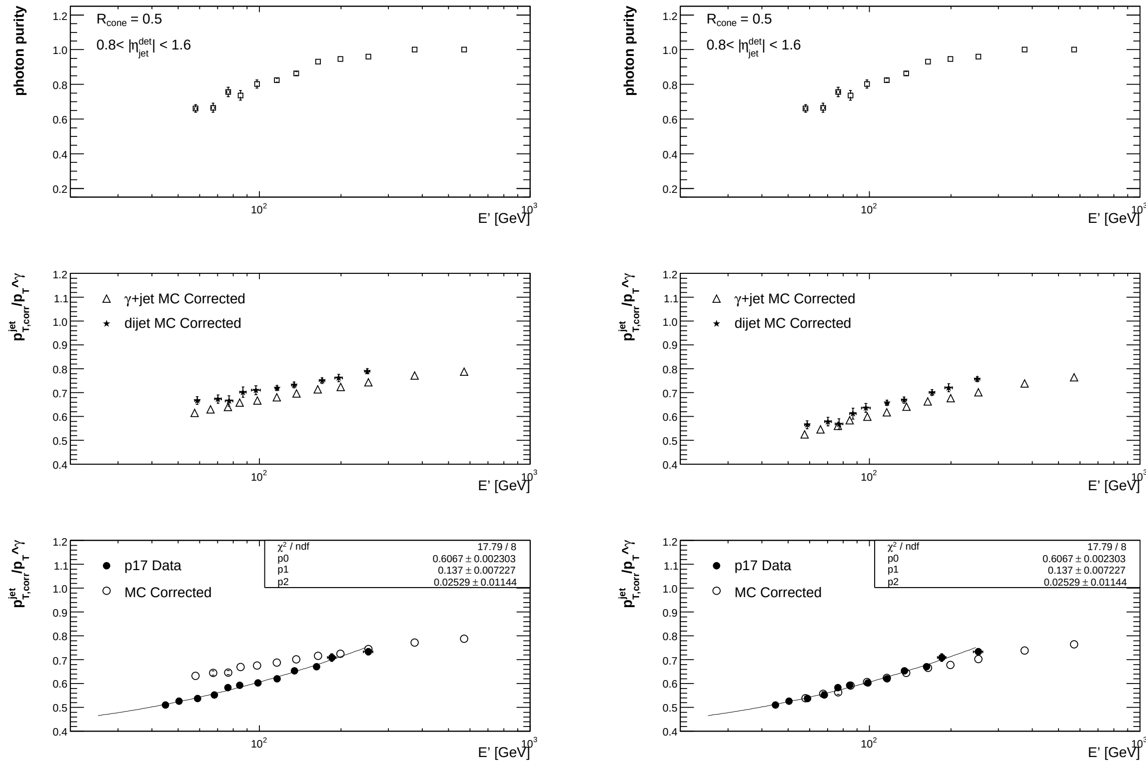

Figure 14: Closure test for MC tuning to data for tight photon selection with $0.8 < |\eta_{det}^{jet}| < 1.6$. Photon purity (top), γ+jet and di-jets MC responses (middle) and combined γ+jet and di-jets MC response compared to data (bottom). Left: default MC; right: MC after tuning.

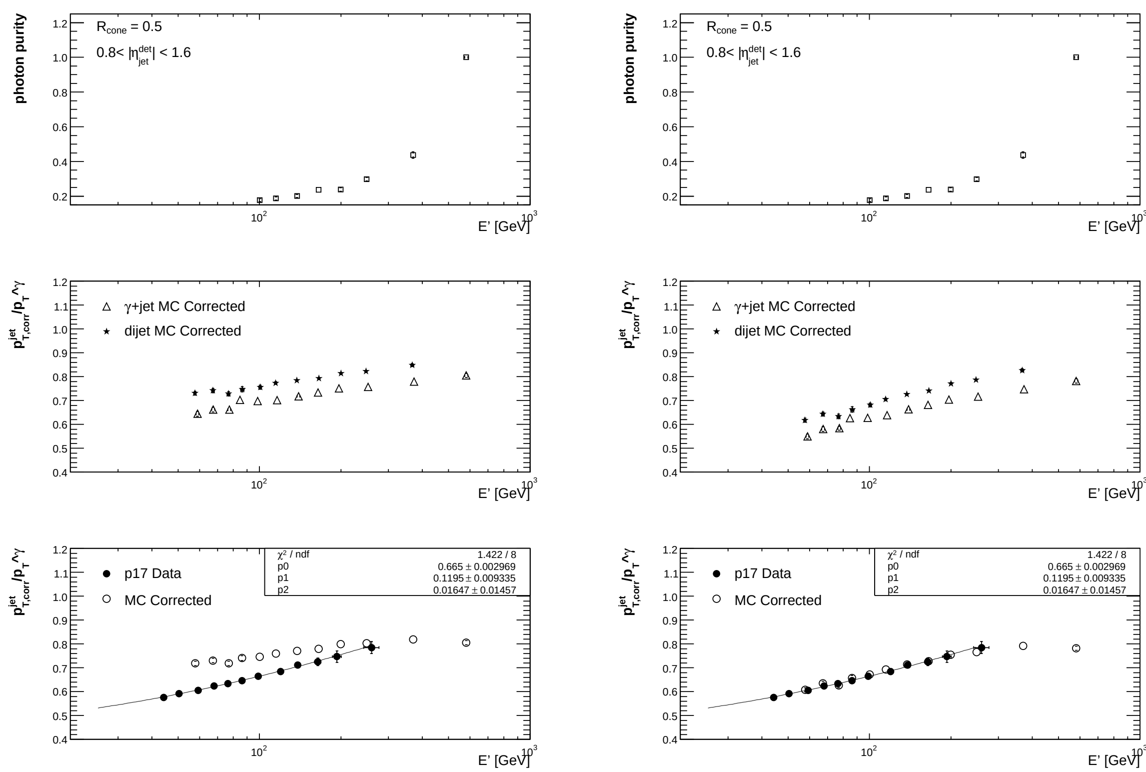

Figure 15: Closure test for MC tuning to data for reversed photon selection with $0.8 < |\eta_{det}^{jet}| < 1.6$. Photon purity (top), γ+jet and di-jets MC responses (middle) and combined γ+jet and di-jets MC response compared to data (bottom). Left: default MC; right: MC after tuning.

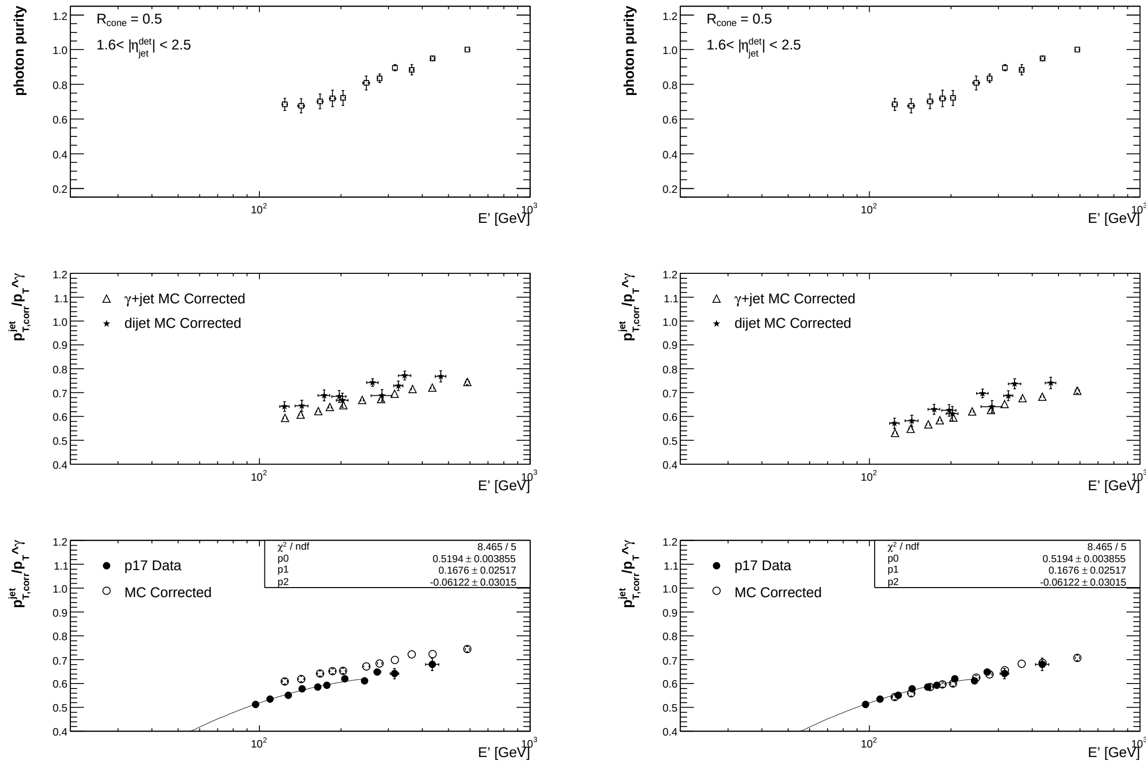

Figure 16: Closure test for MC tuning to data for tight photon selection with $1.6 < |\eta_{det}^{jet}| < 2.5$. Photon purity (top), γ+jet and di-jets MC responses (middle) and combined γ+jet and di-jets MC response compared to data (bottom). Left: default MC; right: MC after tuning.

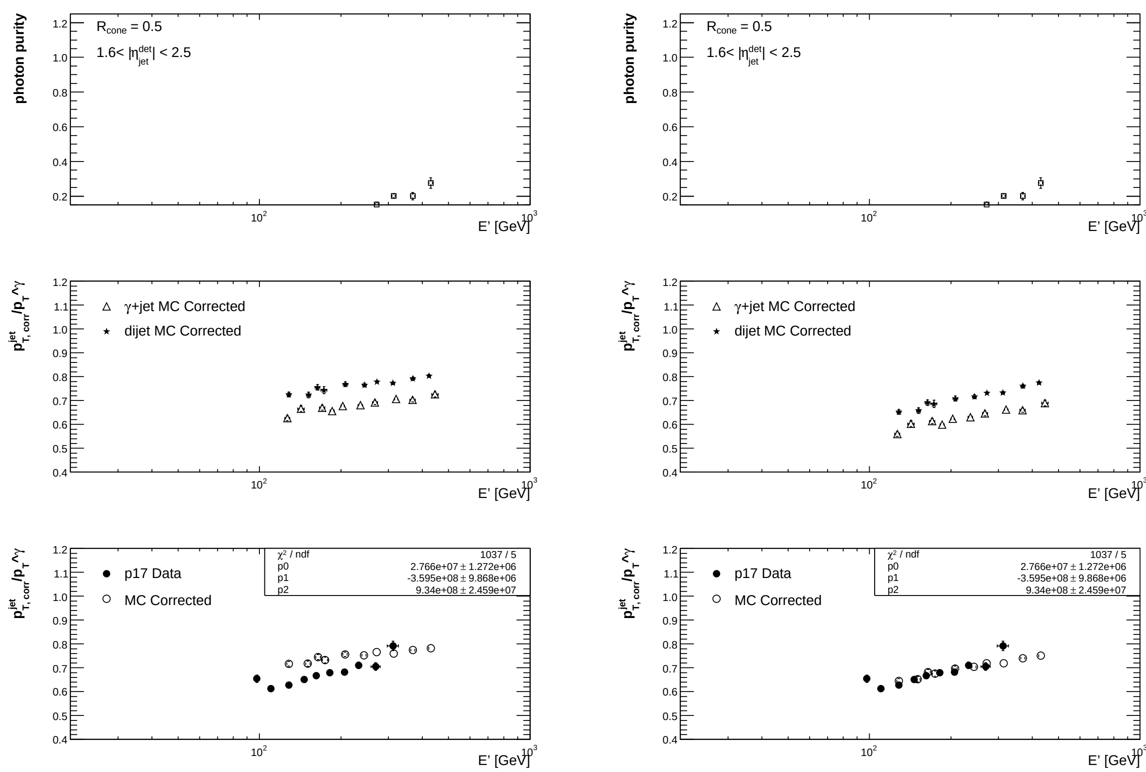

Figure 17: Closure test for MC tuning to data for reversed photon selection with $1.6 < |\eta_{det}^{jet}| < 2.5$. Photon purity (top), γ+jet and di-jets MC responses (middle) and combined γ+jet and di-jets MC response compared to data (bottom). Left: default MC; right: MC after tuning.

5 MC-Data Correction Factor

Using the results obtained in section 3 and 4, we can calculate the MC-data correction factor F defined in Eq. 1. To visualize how large the correction is, we calculate F for different flavors of jets in the γ+jets sample. The results can be seen in Fig. 18. The top row shows the correction factor F for different flavors of jets. The 2nd-4th rows show the ratio between F for different flavors of jets and the averaged F for the jets in the γ+jets sample. The ratios presented in the 2nd-4th rows can be used to correct for the MC-data difference in the jet response for different flavors of jets on average, while at the same time preserves the standard MC JES correction. In order to use these ratios to correct for the MC-data difference for reconstructed calorimeter jets in MC, one needs to determine the flavors of the partons which initiate the jets. One then multiply the JES-corrected jet energy and momentum by the ratios presented in the 2nd-4th rows in Fig. 18. Jets for which one can not find the original parton are most likely coming from ZB overlay and there is no need to apply the above correction for the MC-data difference.

Ultimately one can also use the MC-data correction factor F for each jet. But doing so requires to re-derive the standard JES correction for the γ+jet MC samples corrected for the MC-data difference. This option will be studied in the future.

5.1 Possible Effects on the JSSR

The JSSR [7] is designed to correct for the difference between the MC and data in the jet energy resolution, and the residual jet energy scale effects that are not completely corrected by the standard JES. It has been extracted by comparing γ+jet data and MC, or Z+jet data and MC in terms of the banlance of the transverse momentum of the bosons and jets. After applying the correction for the MC-data difference described in this note, the JSSR needs to be re-examined. From the results presented in [8], we expect that the shifting correction will be largely reduced.

6 Uncertainties

6.1 Residual of the MC Closure Test

As shown in section 3, there are residuals in the MC closure test for the MC single particle responses. The effect on the MC-data correction factor F is studied as the following. Instead of using the MC single particle responses extracted from the single particle MC samples produced with ZS turned off, we use the MC single particle responses from the single particle MC samples produced with ZS turned on. These MC single particle responses with ZS turned on are shown in Fig. 37-46. The corresponding MC closure test results are shown in Fig. 47-51. From these closure test results it is clear that the MC single particle responses with ZS turned on are very different from the ones with ZS turned off. The residuals for the former is much larger than the ones for the latter.

Nevertheless, we obtain very similar MC-data correction factor F using these MC single particle responses with ZS turned on, as shown in Fig. 19. The difference between the results shown in Fig. 18 and the ones in Fig. 19 is assigned as a systematic uncertainty due to the residual seen in the MC closure.

6.2 Electron and Photon Responses in Data

As described in section 4, we assume that the MC simulation has the same electron, photon and muon responses as the ones in data. According to [6], the electron energy scale uncertainty is 0.3% by comparing the extracted Z mass in the two electron final state between the data and MC. Since electrons lose more energy in dead material than photons, the electron energy scale corrections effectively "overcorrect" the photon energies, so another 0.5% photon-to-electron energy scale uncertainty is also taken into account according to [2]. We use the quadrature of the above two uncertainties as the photon energy scale uncertainty, 0.58%. We repeat the extraction of the single particle data responses as described in section 4 but with:

$$R_{\gamma}^{data} = (1 \pm 0.0058) \cdot R_{\gamma}^{MC}, \quad (14)$$

$$R_{e^{\pm}}^{data} = (1 \pm 0.003) \cdot R_{e^{\pm}}^{MC}, \quad (15)$$

The obtained MC-data correction factor F are shown in Fig. 20. The change in the estimated MC-data correction factor F is assigned as a systematic uncertainty.

6.3 Data Single Hadron Responses

The uncertainties on the parameters A, B and C shown in Fig. 8-9 are propagated to the MC-data correction factor F.

6.4 Combined Systematic Uncertainty

The total systematic uncertainty is given by the quadrature sum of the above three contributions. The results for the ratios between F for different flavors of jets and the averaged F for the γ+jets sample are shown in Fig. 21.

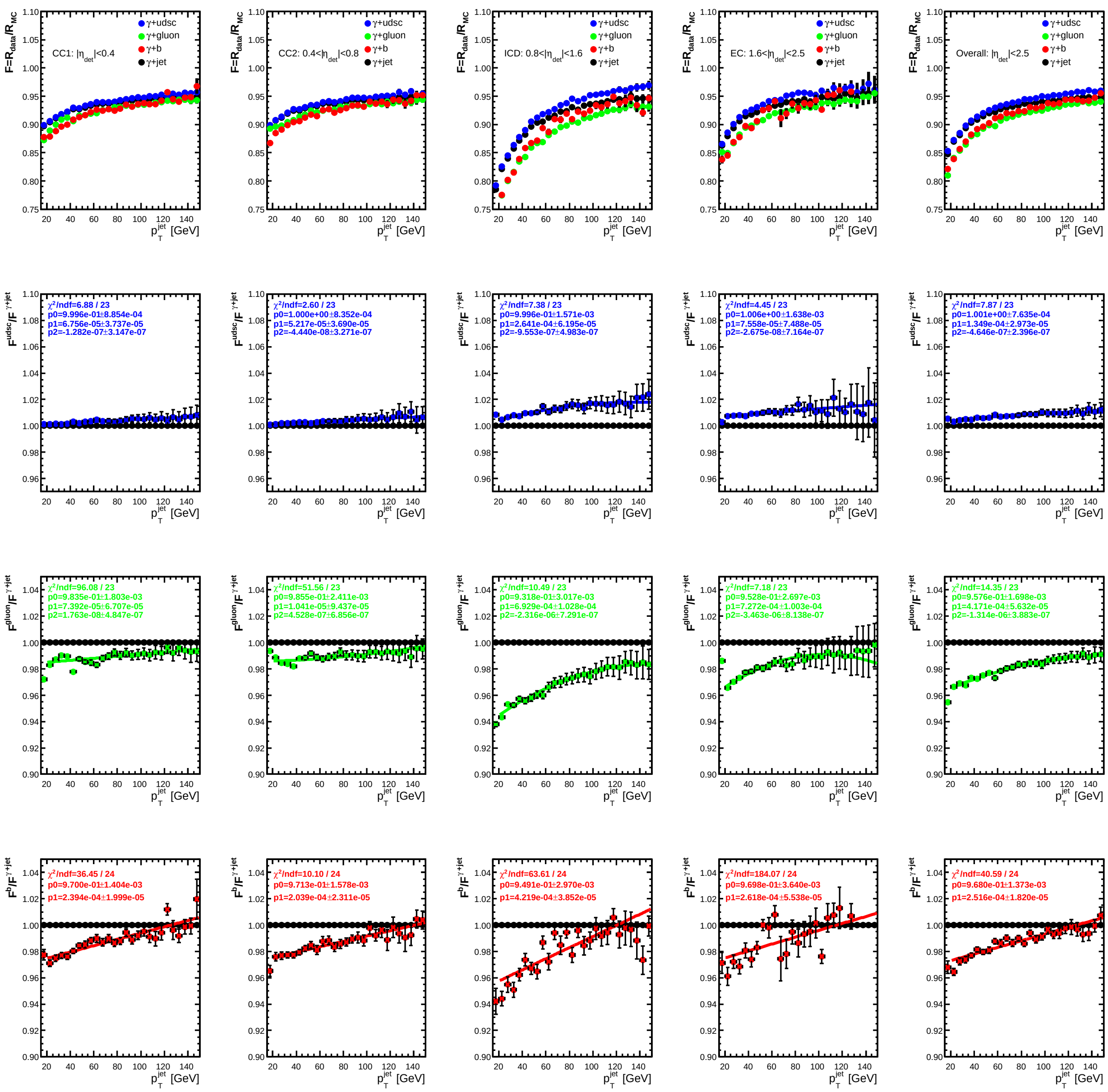

Figure 18: MC-data correction factor F estimated for jets with different flavors in γ+jet MC samples. The MC single particle responses used here are extracted from the single particle MC samples with ZS turned off. Top: the correction factor F for light flavor quark jets (blue), gluon jets (green), b quark jets (red) and the averaged F for the γ+jets sample (black). The 2nd-4th rows show the ratio between F for different flavors of jets and the averaged F for the γ+jets sample.

7 Conclusion

We present a method to correct for the MC-data difference in the jet response at DØ so that the corrected MC has the same kinematic and flavor-dependent jet response as that in the data. The method use the spatially matched particle jet, MC and data single particle responses.to obtain the MC-data correction factor. The MC single particle responses are extracted from single particle MC samples. The data single particle responses are extracted by tuning MC jet responses through underlying single particle responses so that they match the data jet response. Results for Run IIA MC and data JCCB jets are presented, including flavor-dependent MC-data correction factors that preserve the standard JES for the MC.

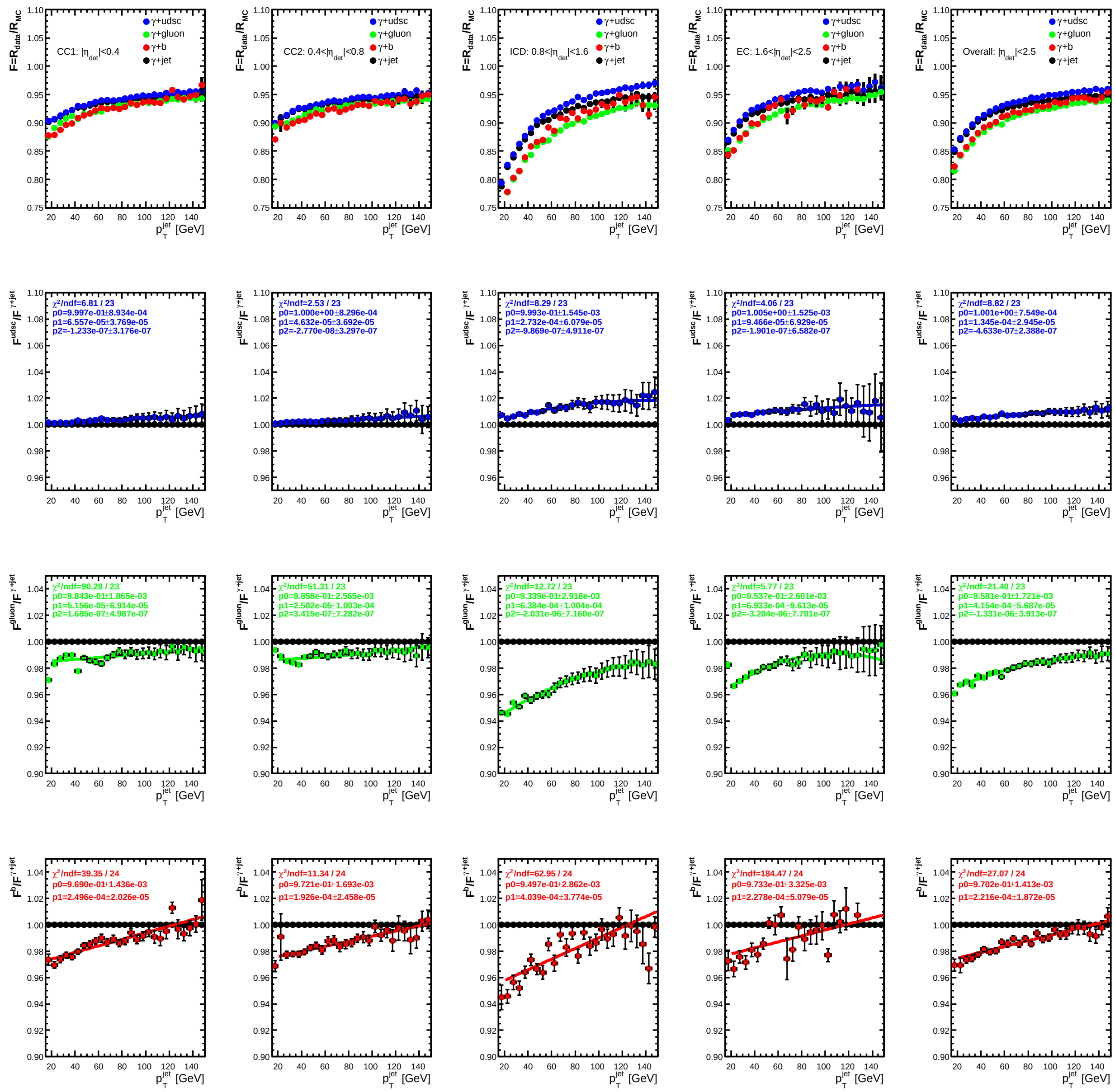

Figure 19: Same as Fig. 18 but the MC single particle responses used here are extracted from the single particle MC samples with ZS turned on.

Acknowledgments

We thank Dmitri Bandurin, Leo Bellantoni, Dan Boline, Fabrice Couderc, Frederic Deliot, Georgy Golovanov, Gaston Gutierrez, Shabnam Jabeen, Alexandr Kupco, Amnon Harel, Yvonne Peters, Peter Renkel, Viatcheslav Sharyy, Jan Stark, Peter Svoisky and many others for their valuable suggestions and help.

References

[1] A. Bhatti et al., Determination of the Jet Energy Scale at the Collider Detector at Fermilab, Nucl. Instrum. Meth. A 566 (2006) 375.

[2] Jet Energy Scale Determination at DØ Run II, DØ note 5382.

[3] Z. Ye et al., Measurement of the Top Quark Mass in the Lepton+Jets Channel Using the Matrix Element Method on 3.6 fb^{-1} DØ Run II Data, DØ note 5877.

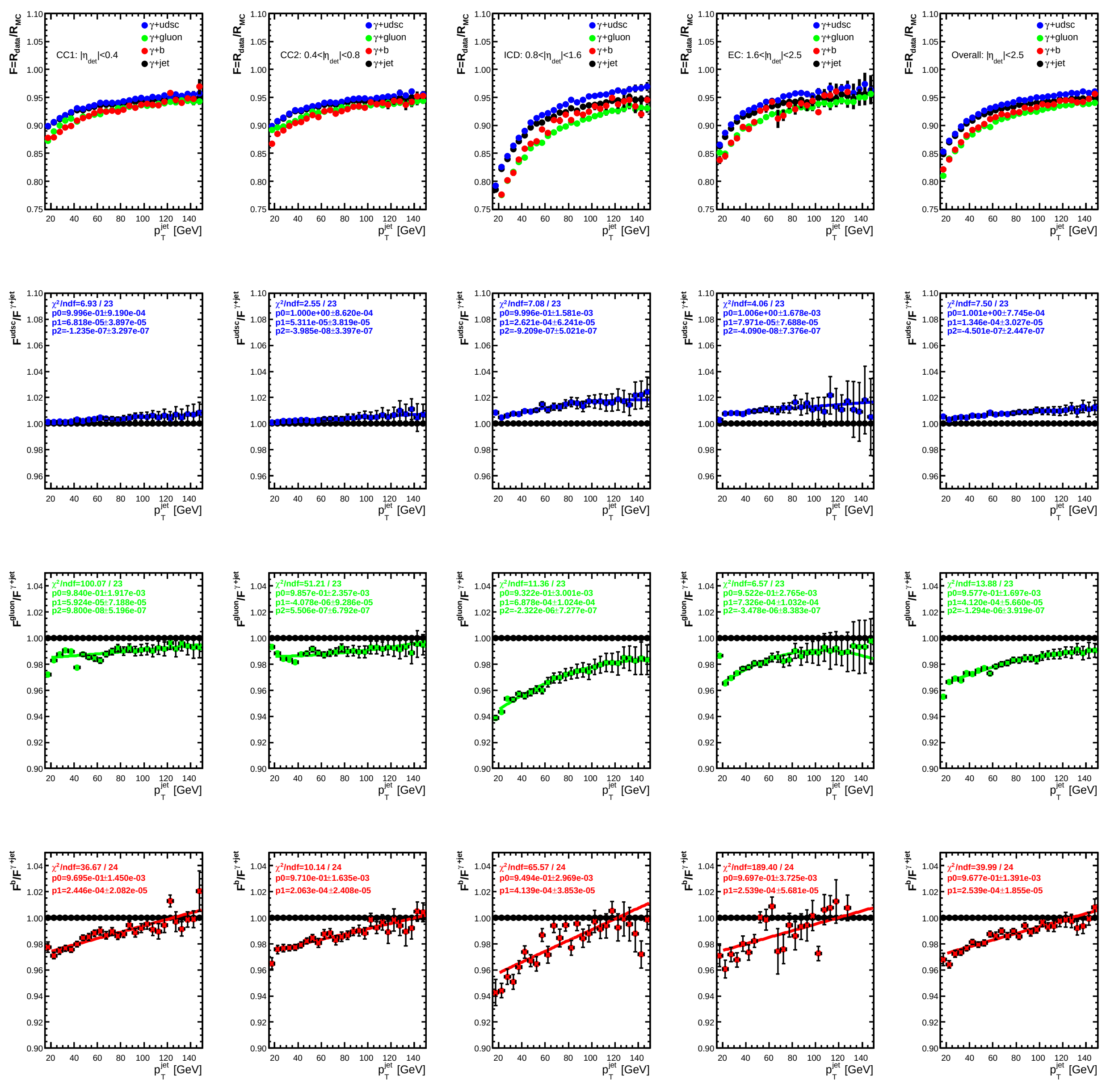

Figure 20: Same as Fig. 18 but we use the photon and electron responses in data given in Eq. 14 and 15.

[4] A. Harel, An estimate of the data over MC, b over light jet response uncertainty for Run IIA JES, DØ note 5654.

[5] D. Boline, Sample Dependent Correction to the Jet Energy Scale, DØ note 5572.

[6] X. Bu et al., DØ Note 5846.

[7] N. Makovec and J. Grivaz, Shifting, Smearing and Removing Simulated Jets, DØ note 4914.

[8] C. Orchando and J. Grivaz, SSR for quarks and gluons, talk given in the DØ JES meeting on May 15, 2008.

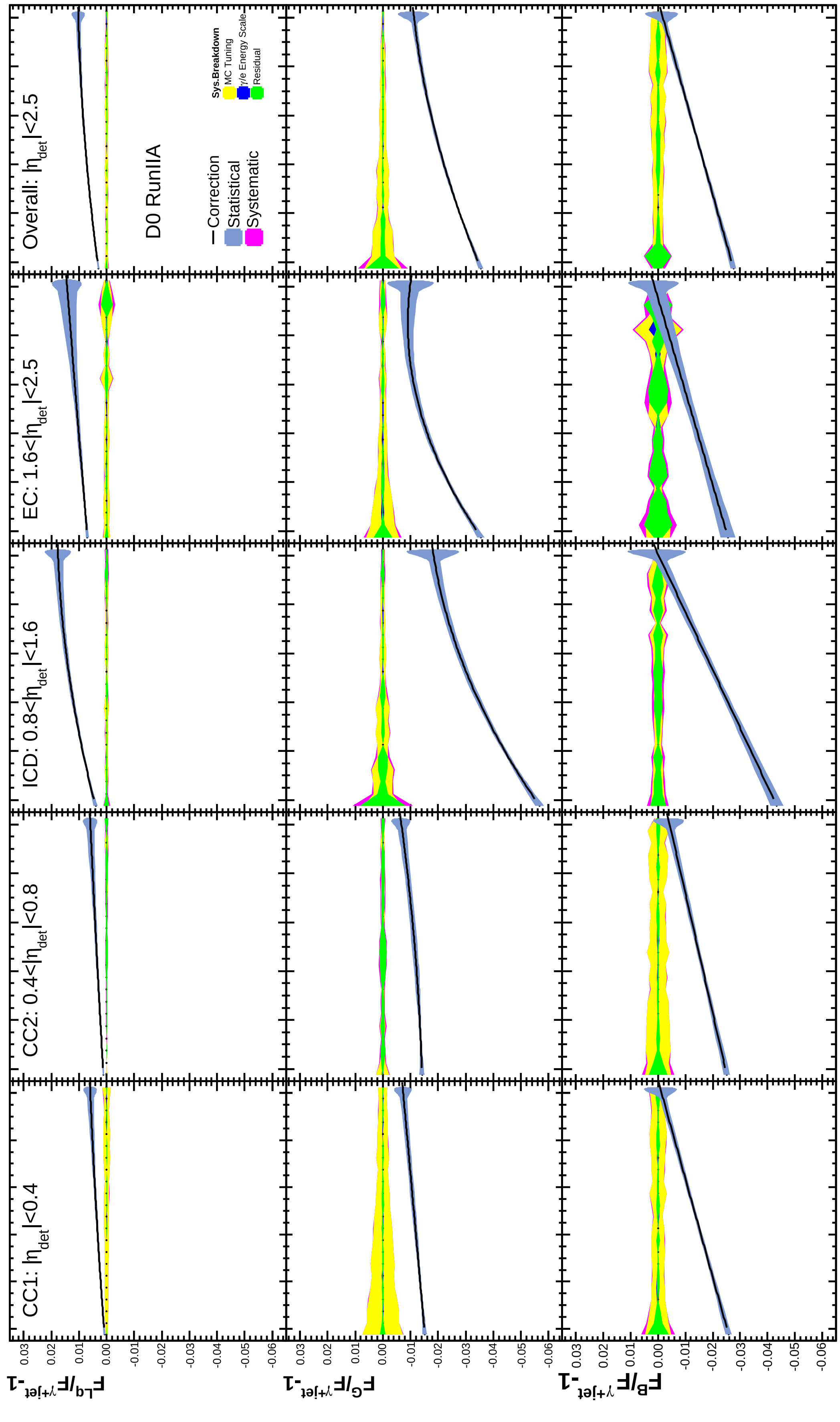

Figure 21: Correction factor for MC-data difference in the jet response for different flavors of jets for Run IIA. They are given by the ratios between F for different flavors of jets and the averaged F for the γ+jets sample.

A MC Single Particle Responses From Single Particle MC Samples Produced With Zero Suppression Turned Off

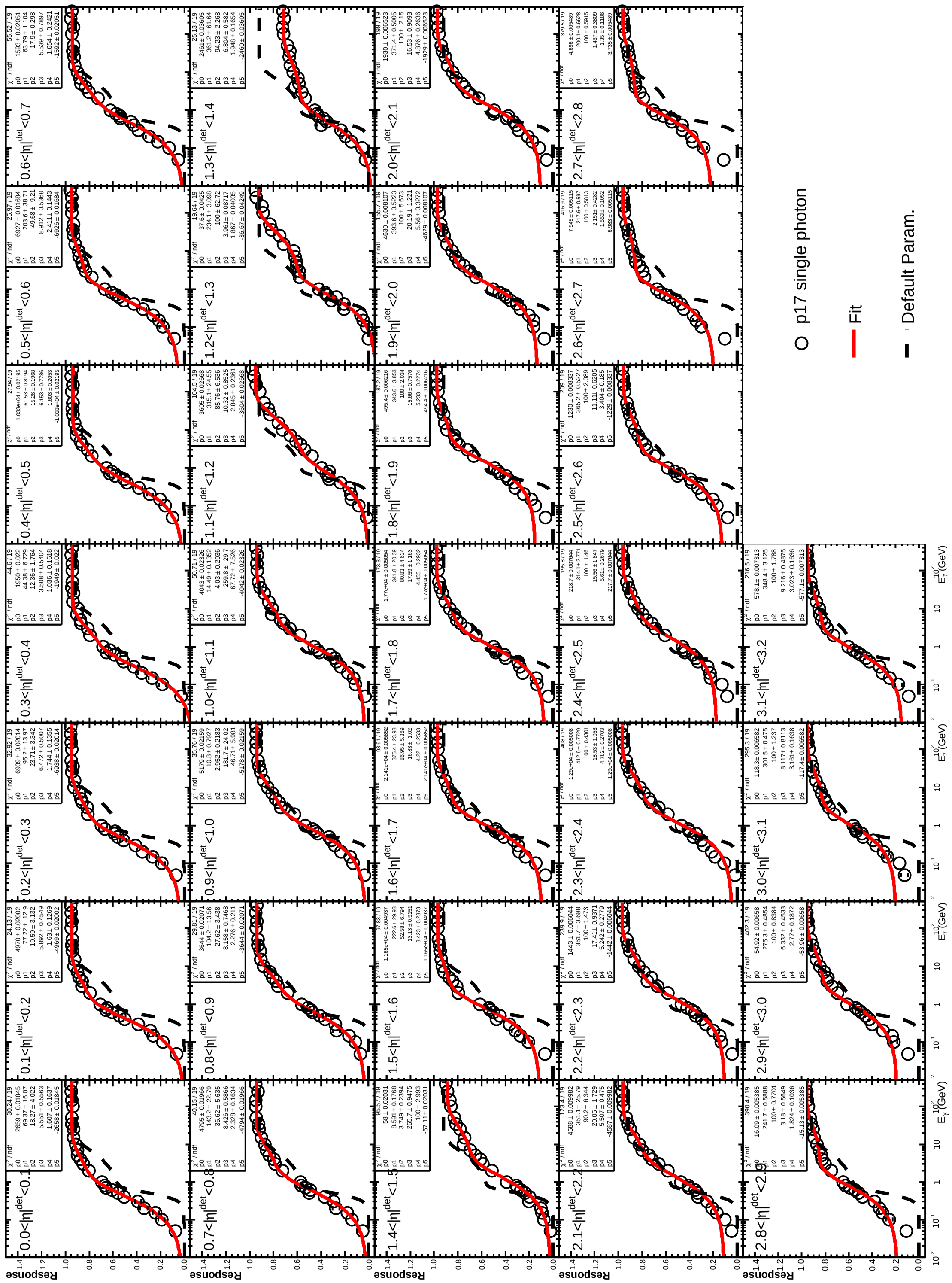

Figure 22: MC single photon response from p17 single γ MC sample, produced without ZS, calorimeter noise or ZB overlay. The black dashed line corresponds to the single photon response from Run IIA W mass studies. The red line is a fit to the MC points in black circles.

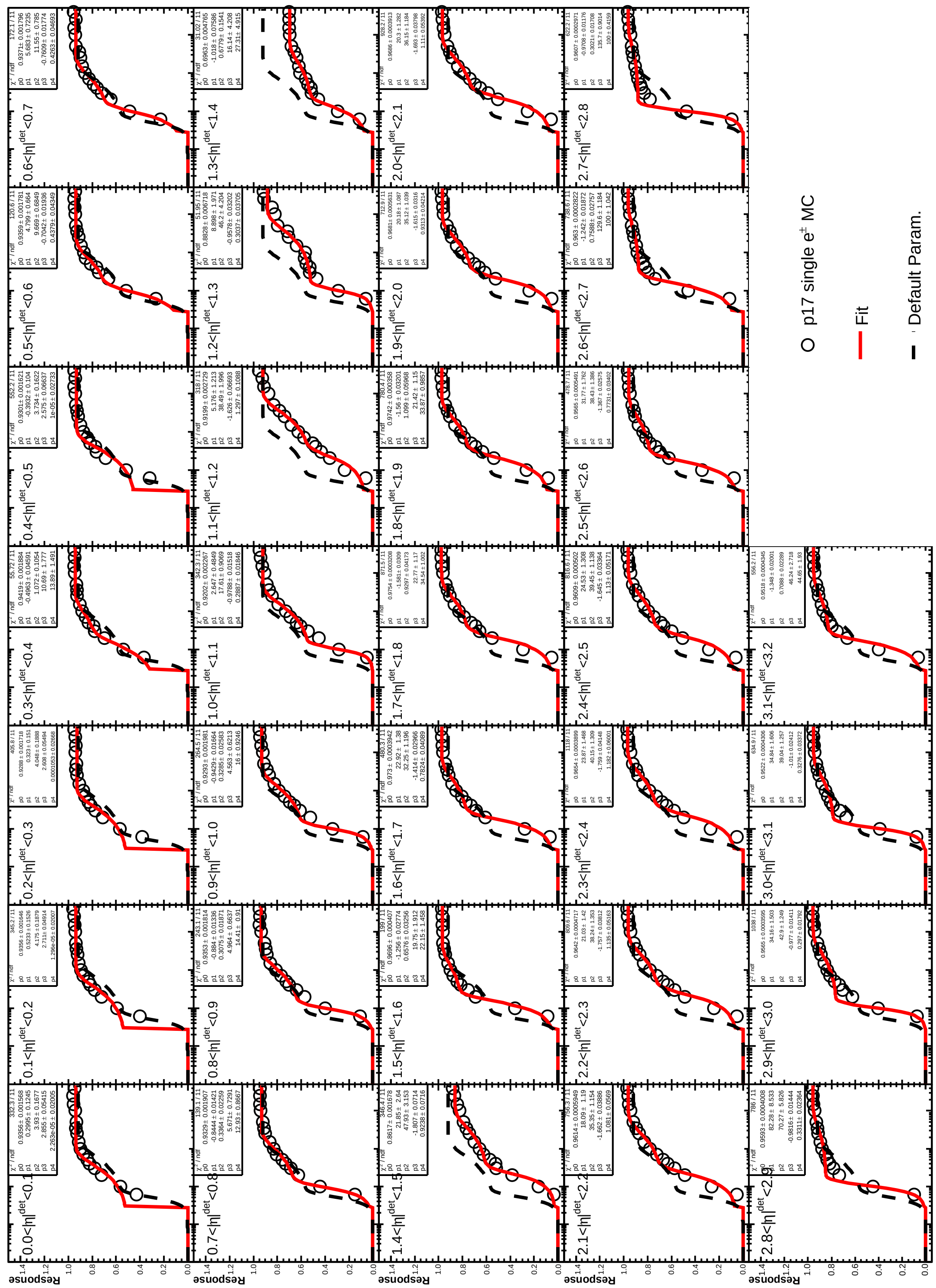

Figure 23: MC single electron response from p17 single $e^{\pm}$ MC sample, produced without ZS, calorimeter noise or ZB overlay. The black dashed line corresponds to the single electron response from Run IIA W mass studies. The red line is a fit to the MC points in black circles.

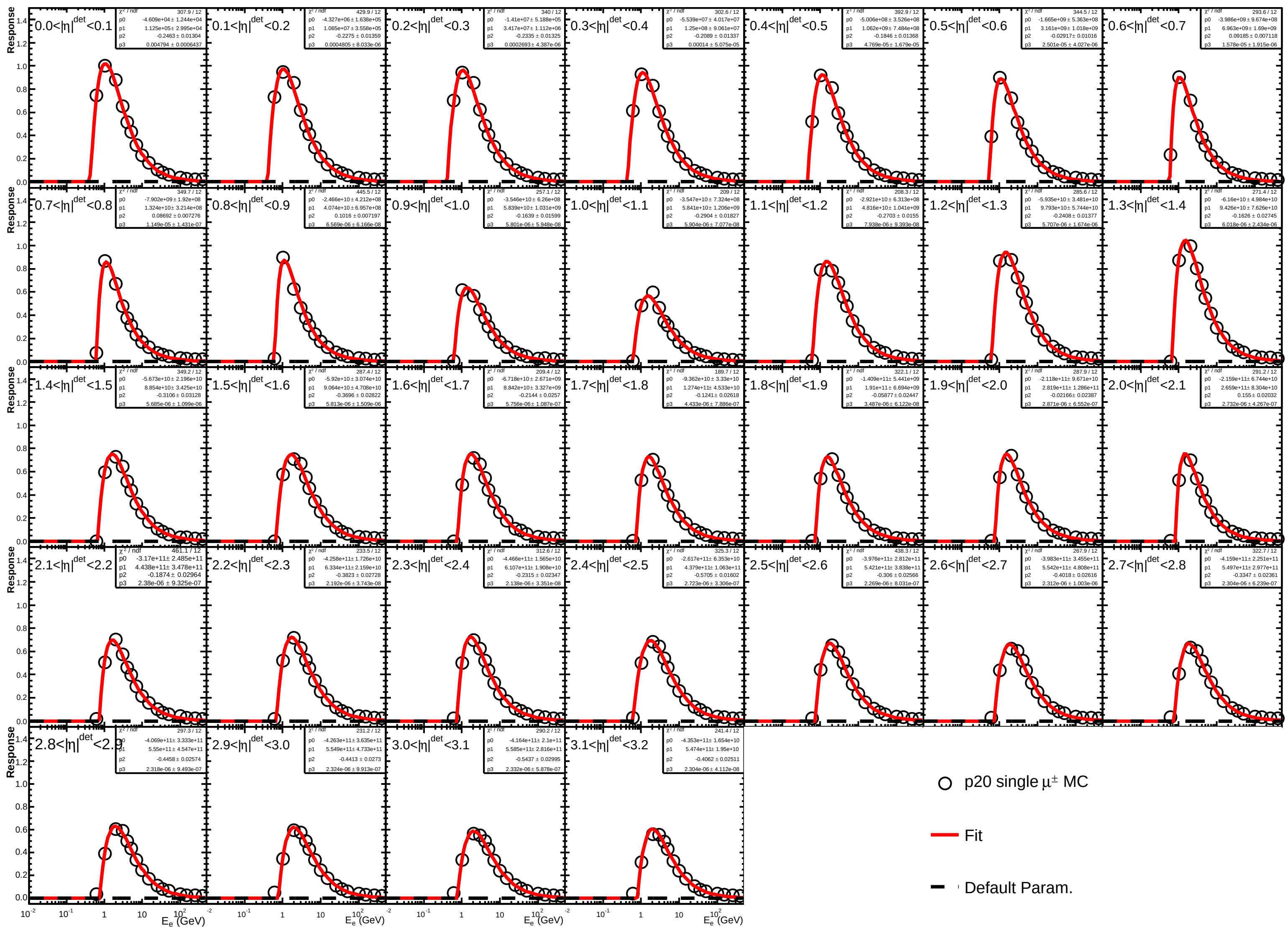

Figure 24: MC single electron response from p17 single $\mu^{\pm}$ MC sample, produced without ZS, calorimeter noise or ZB overlay. The black dashed line corresponds to 0. The red line is a fit to the MC points in black circles.

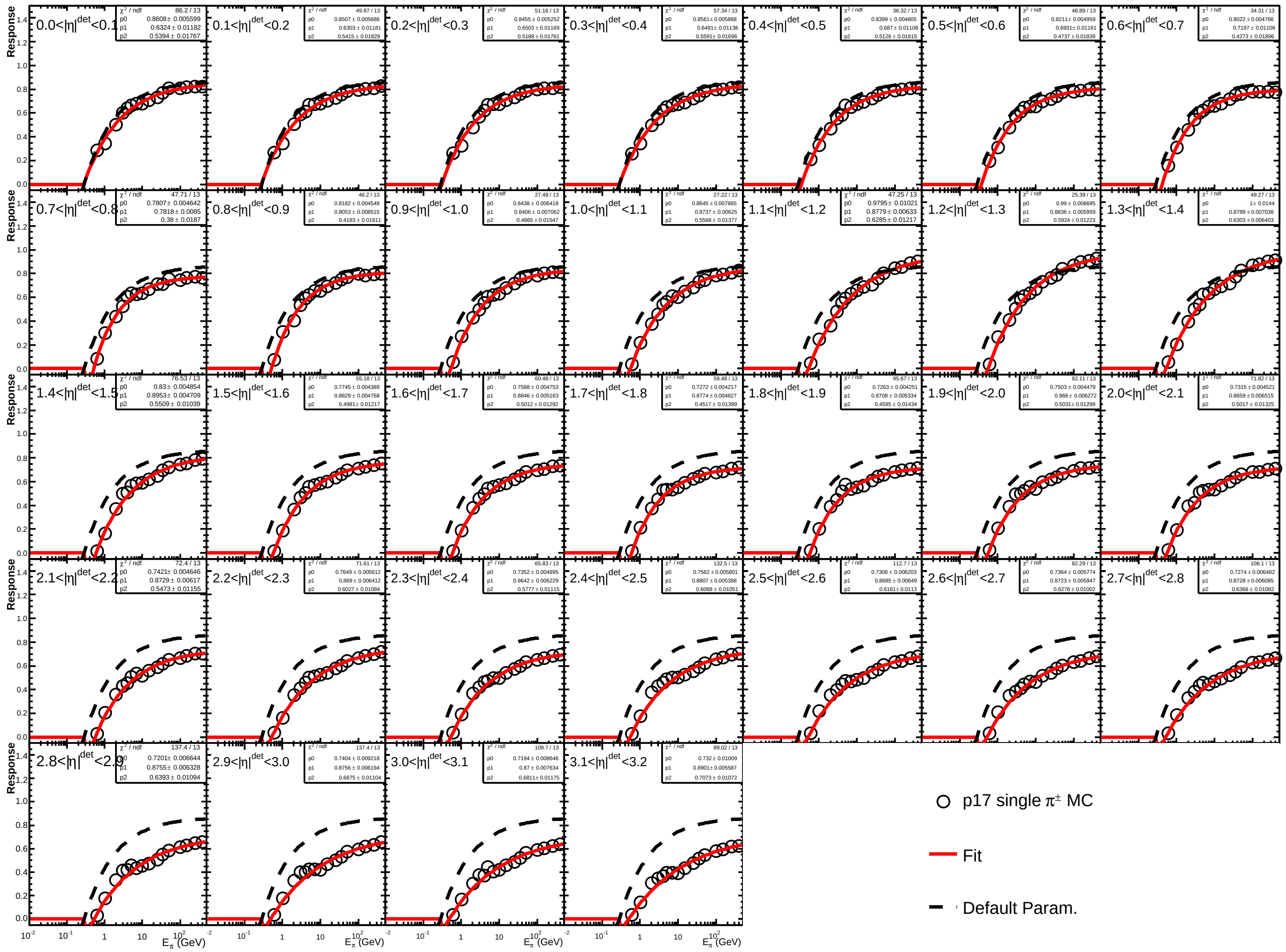

Figure 25: MC single pion response from p17 single $\pi^{\pm}$ MC sample, produced without ZS, calorimeter noise or ZB overlay. The black dashed line corresponds to the single pion response from Run IIA JES studies. The red line is a fit to the MC points in black circles.

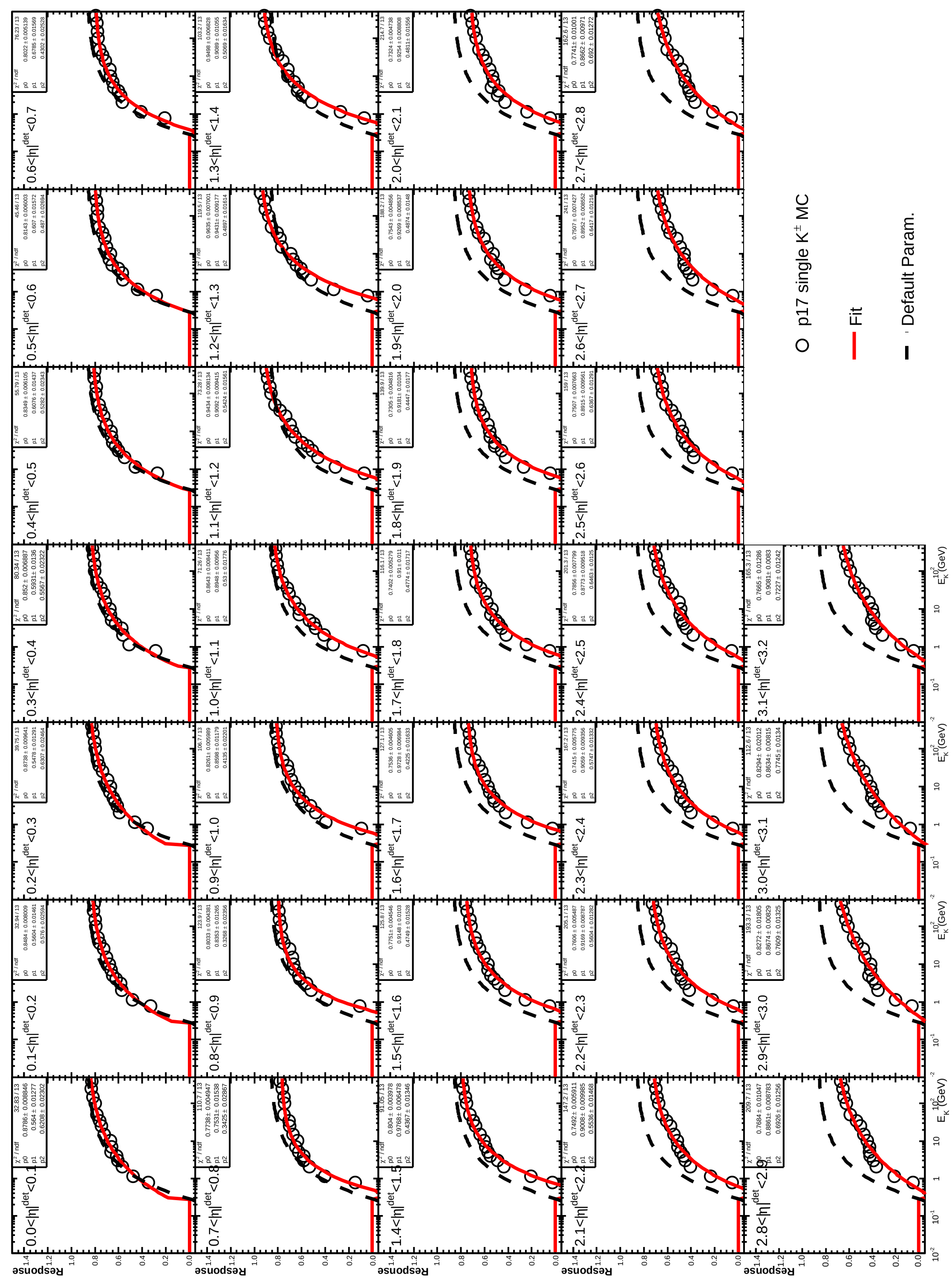

Figure 26: MC single kaon response from p17 single $K^{\pm}$ MC sample, produced without ZS, calorimeter noise or ZB overlay. The black dashed line corresponds to the single pion response from Run IIA JES studies. The red line is a fit to the MC points in black circles.

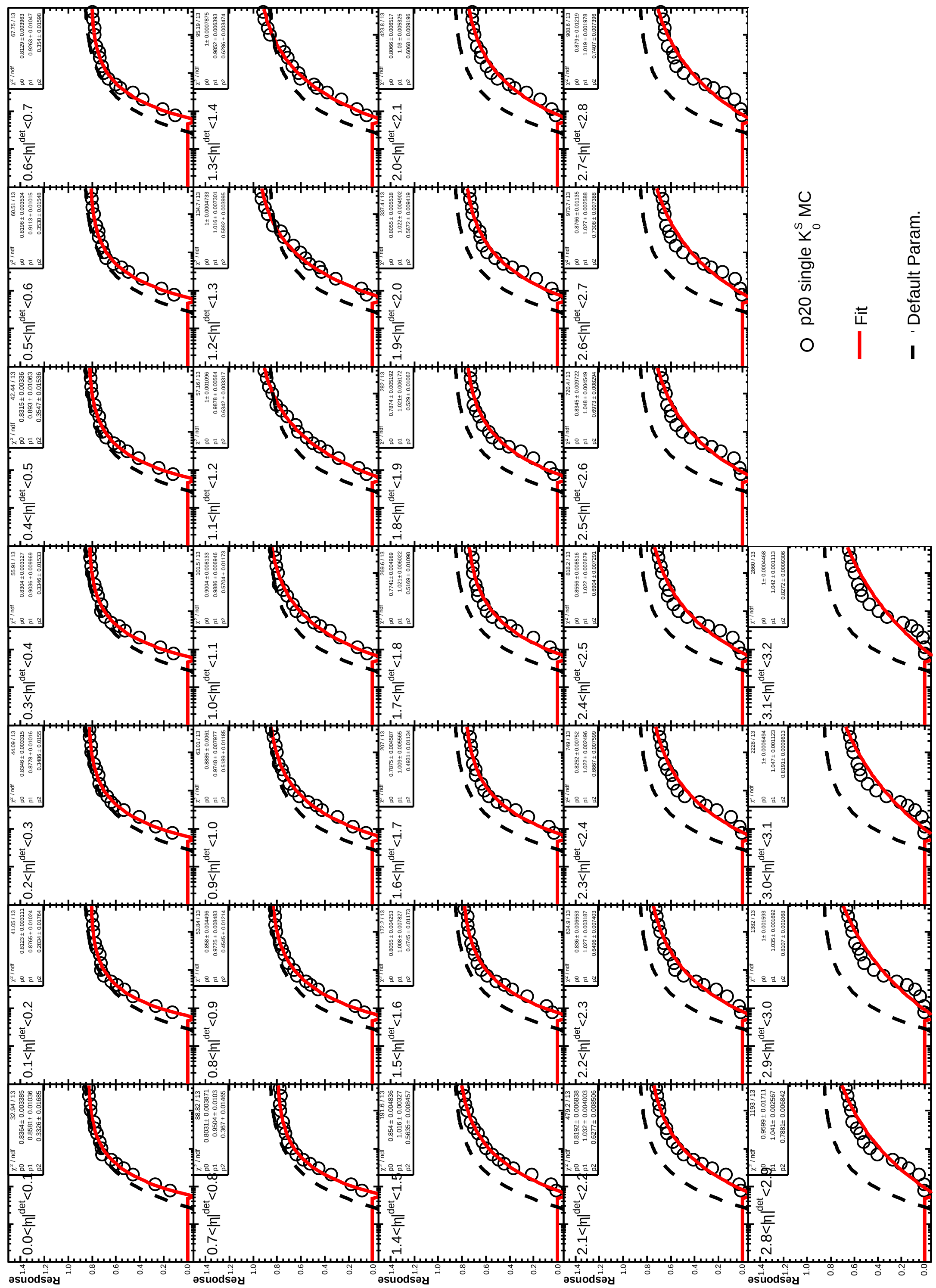

Figure 27: MC single kaon response from p17 single K_0^S MC sample, produced without ZS, calorimeter noise or ZB overlay. The black dashed line corresponds to the single pion response from Run IIA JES studies. The red line is a fit to the MC points in black circles.

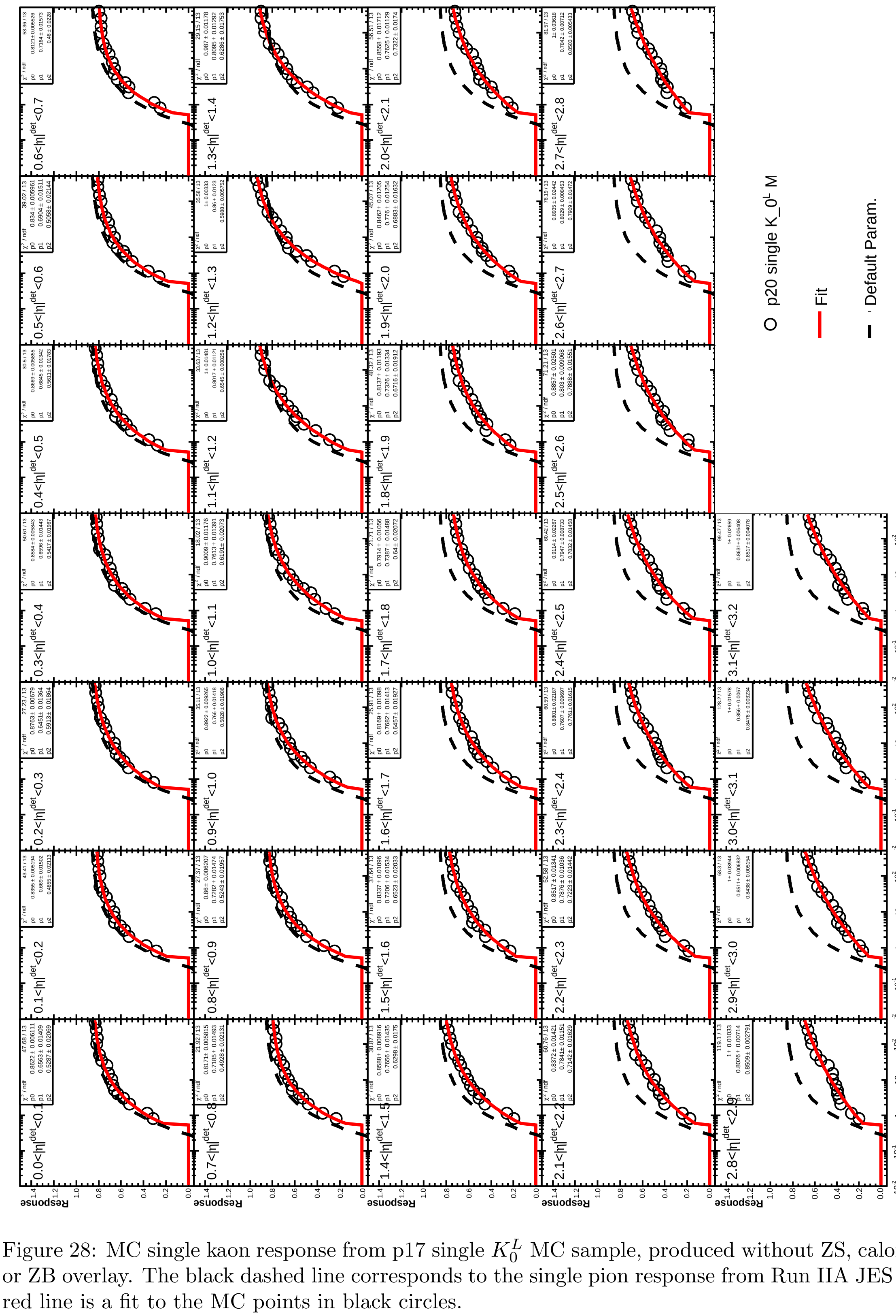

Figure 28: MC single kaon response from p17 single K_0^L MC sample, produced without ZS, calorimeter noise or ZB overlay. The black dashed line corresponds to the single pion response from Run IIA JES studies. The red line is a fit to the MC points in black circles.

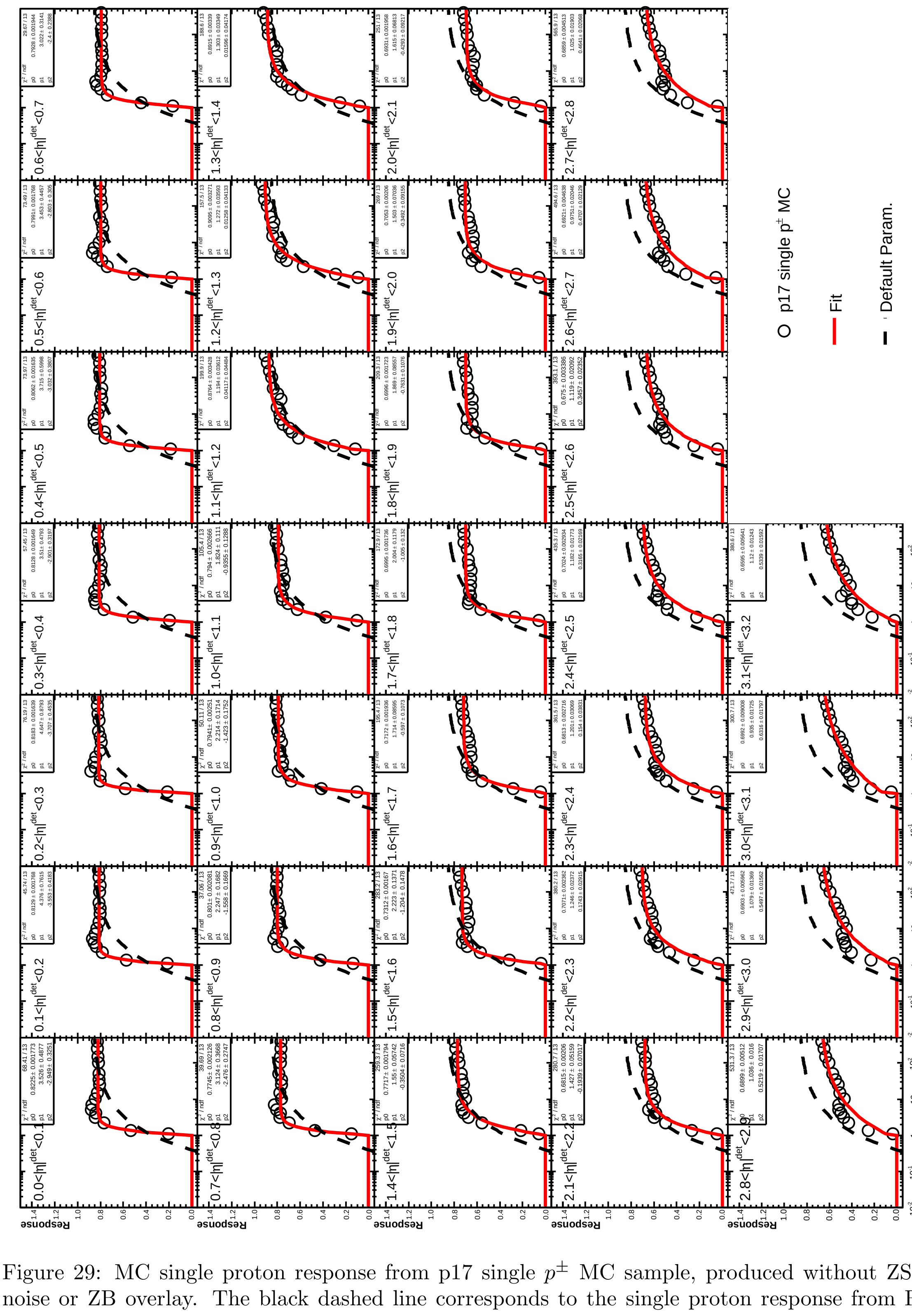

Figure 29: MC single proton response from p17 single $p^{\pm}$ MC sample, produced without ZS, calorimeter noise or ZB overlay. The black dashed line corresponds to the single proton response from Run IIA JES studies. The red line is a fit to the MC points in black circles.

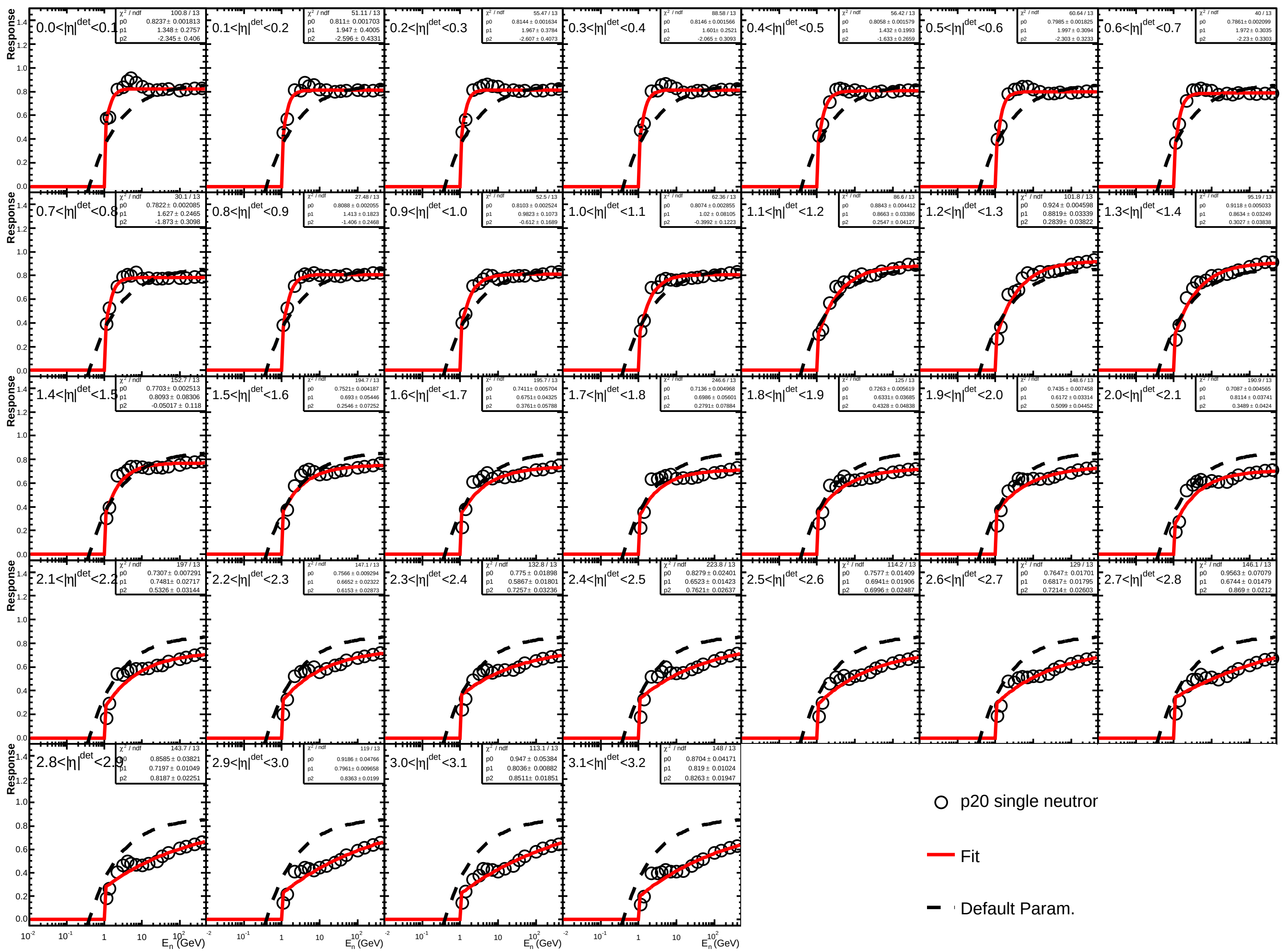

Figure 30: MC single proton response from p17 single n MC sample, produced without ZS, calorimeter noise or ZB overlay. The black dashed line corresponds to the single proton response from Run IIA JES studies. The red line is a fit to the MC points in black circles.

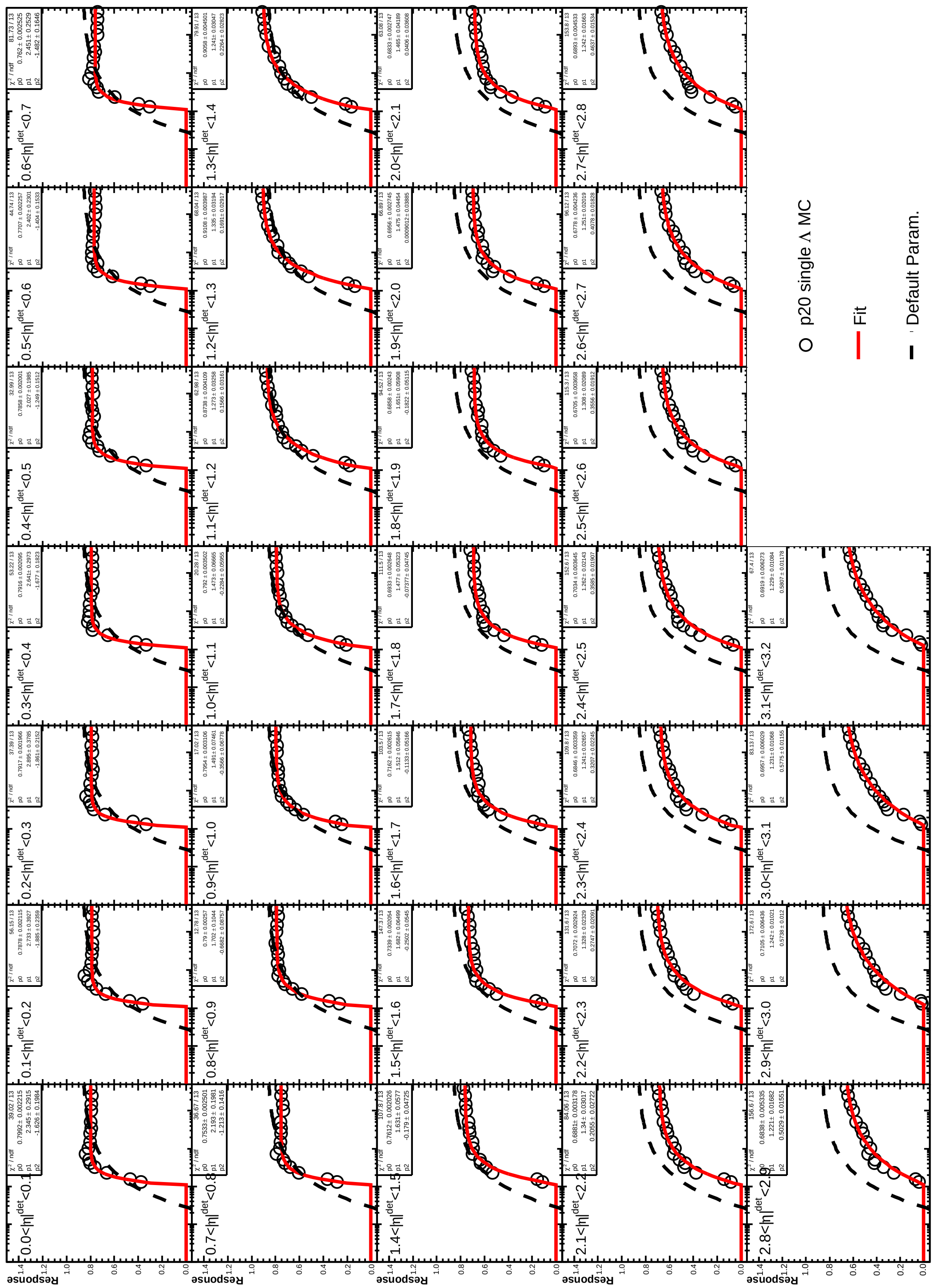

Figure 31: MC single proton response from p17 single Λ MC sample, produced without ZS, calorimeter noise or ZB overlay. The black dashed line corresponds to the single pion response from Run IIA JES studies. The red line is a fit to the MC points in black circles.

B MC Closure Test on γ+jet MC Samples Produced Without ZB overlay

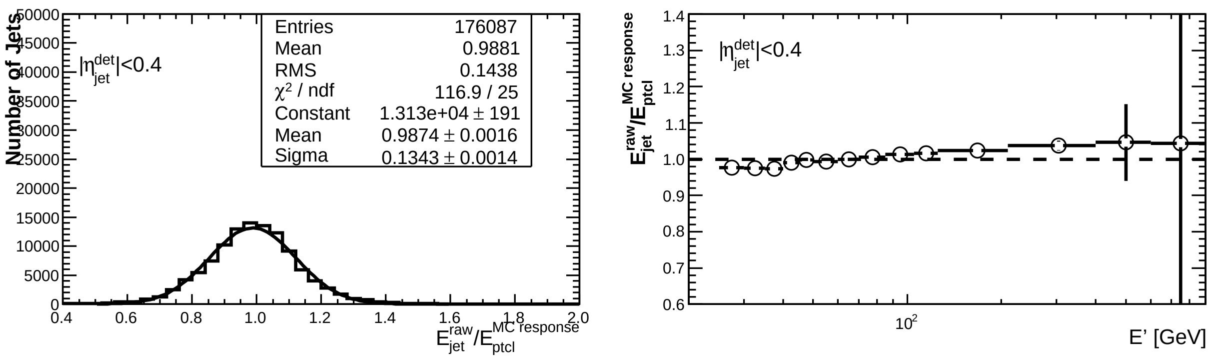

Figure 32: MC closure test for jets in p17 γ+jet MC sample produced without ZB overlay for $|\eta_{det}^{jet}| < 0.4$. The single particle MC responses are derived with ZS turned off. The offset corrections are not included. The x-axis E' is given by $p_T^{\gamma} \cdot cosh(\eta^{jet})$.

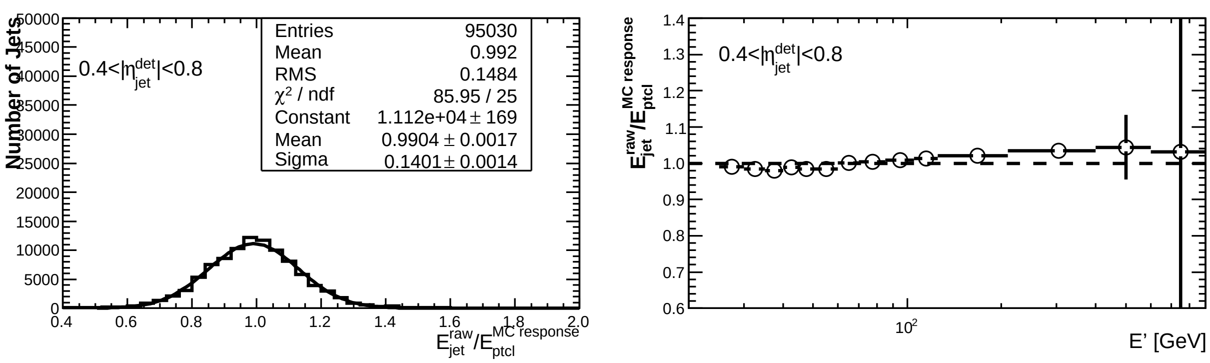

Figure 33: MC closure test for jets in p17 γ+jet MC sample produced without ZB overlay for $0.4 < |\eta_{det}^{jet}| < 0.8$. The single particle MC responses are derived with ZS turned off. The offset corrections are not included. The x-axis E' is given by $p_T^{\gamma} \cdot cosh(\eta^{jet})$.

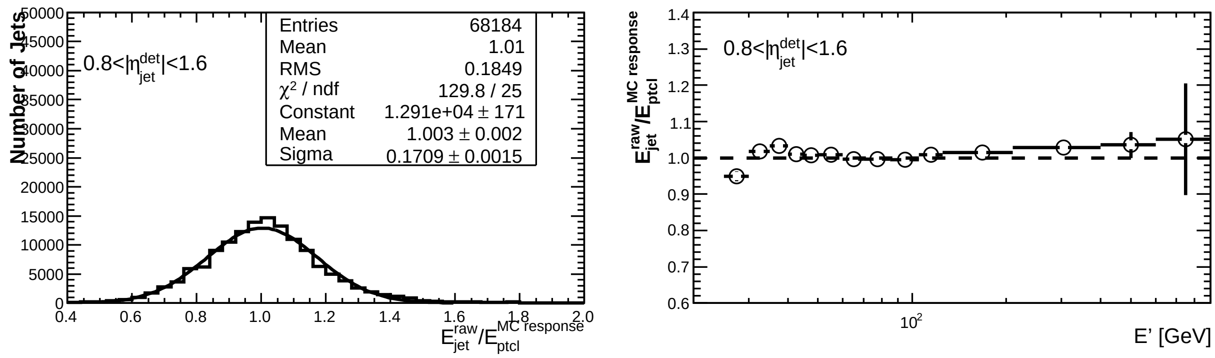

Figure 34: MC closure test for jets in p17 γ+jet MC sample produced without ZB overlay for $0.8 < |\eta_{det}^{jet}| < 1.6$. The single particle MC responses are derived with ZS turned off. The offset corrections are not included. The x-axis E' is given by $p_T^{\gamma} \cdot cosh(\eta^{jet})$.

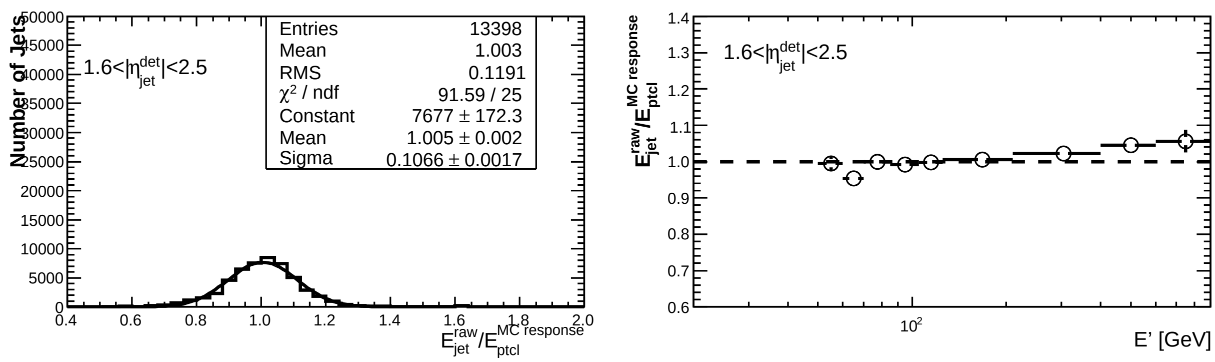

Figure 35: MC closure test for jets in p17 γ+jet MC sample produced without ZB overlay for $1.6 < |\eta_{det}^{jet}| < 2.5$. The single particle MC responses are derived with ZS turned off. The offset corrections are not included. The x-axis E' is given by $p_T^{\gamma} \cdot cosh(\eta^{jet})$.

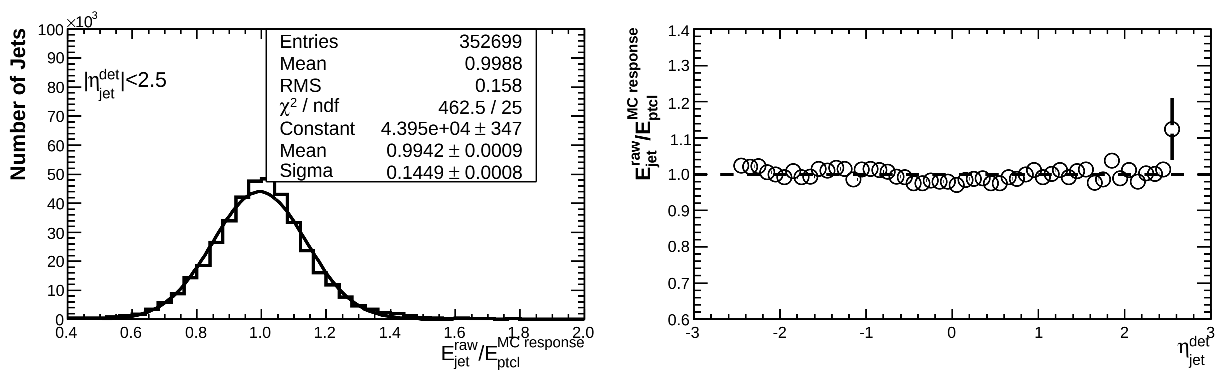

Figure 36: MC closure test for jets in p17 γ+jet MC sample produced without ZB overlay for $|\eta_{det}^{jet}| < 2.5$. The single particle MC responses are derived with ZS turned off. The offset corrections are not included. The x-axis E' is given by $p_T^{\gamma} \cdot cosh(\eta^{jet})$.

C MC Single Particle Responses From Single Particle MC Samples Produced With Zero Suppression Turned On

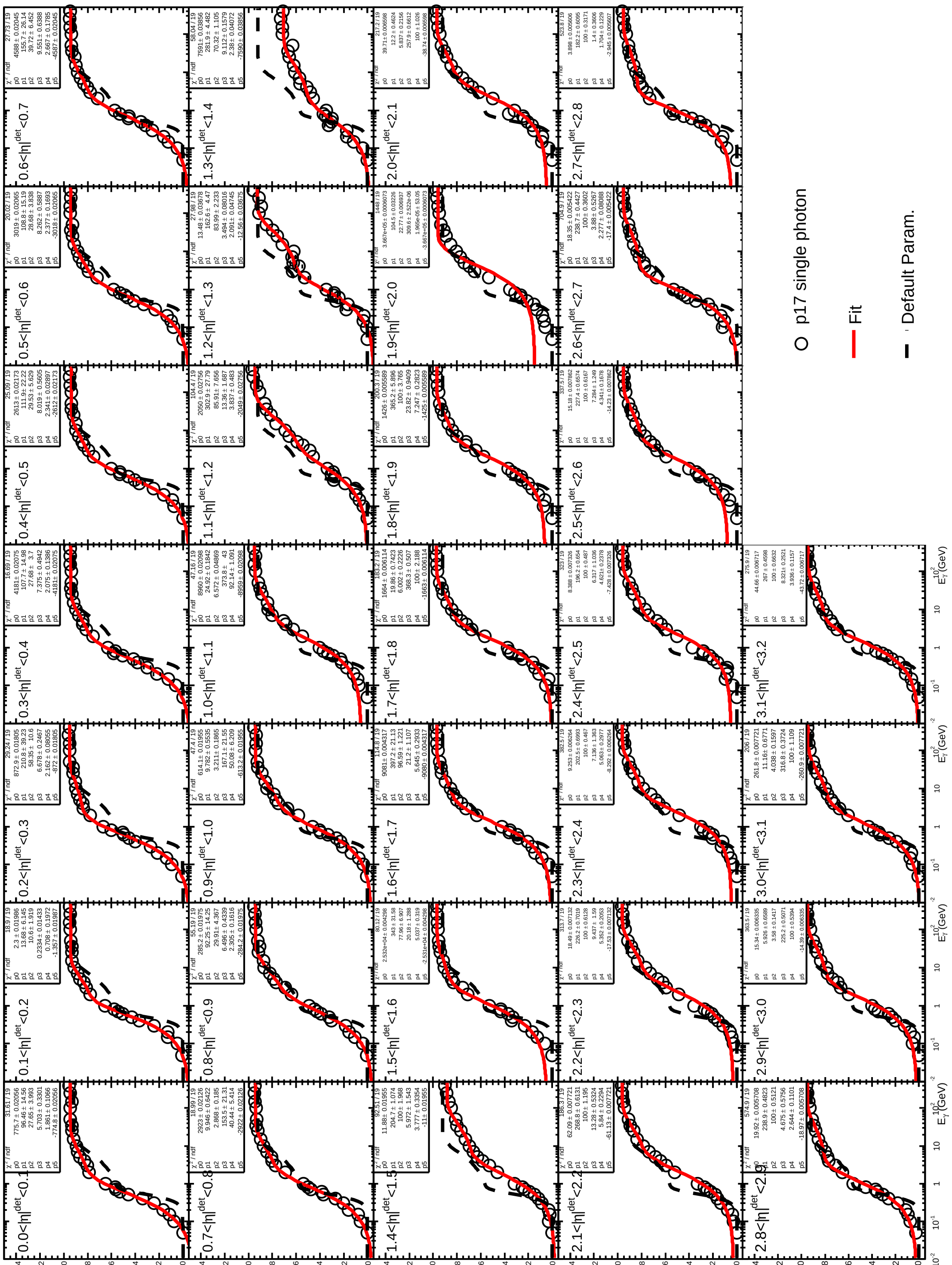

Figure 37: MC single photon response from p17 single γ MC sample, produced with ZS turned on. The black dashed line corresponds to the single photon response from Run IIA W mass studies. The red line is a fit to the MC points in black circles.

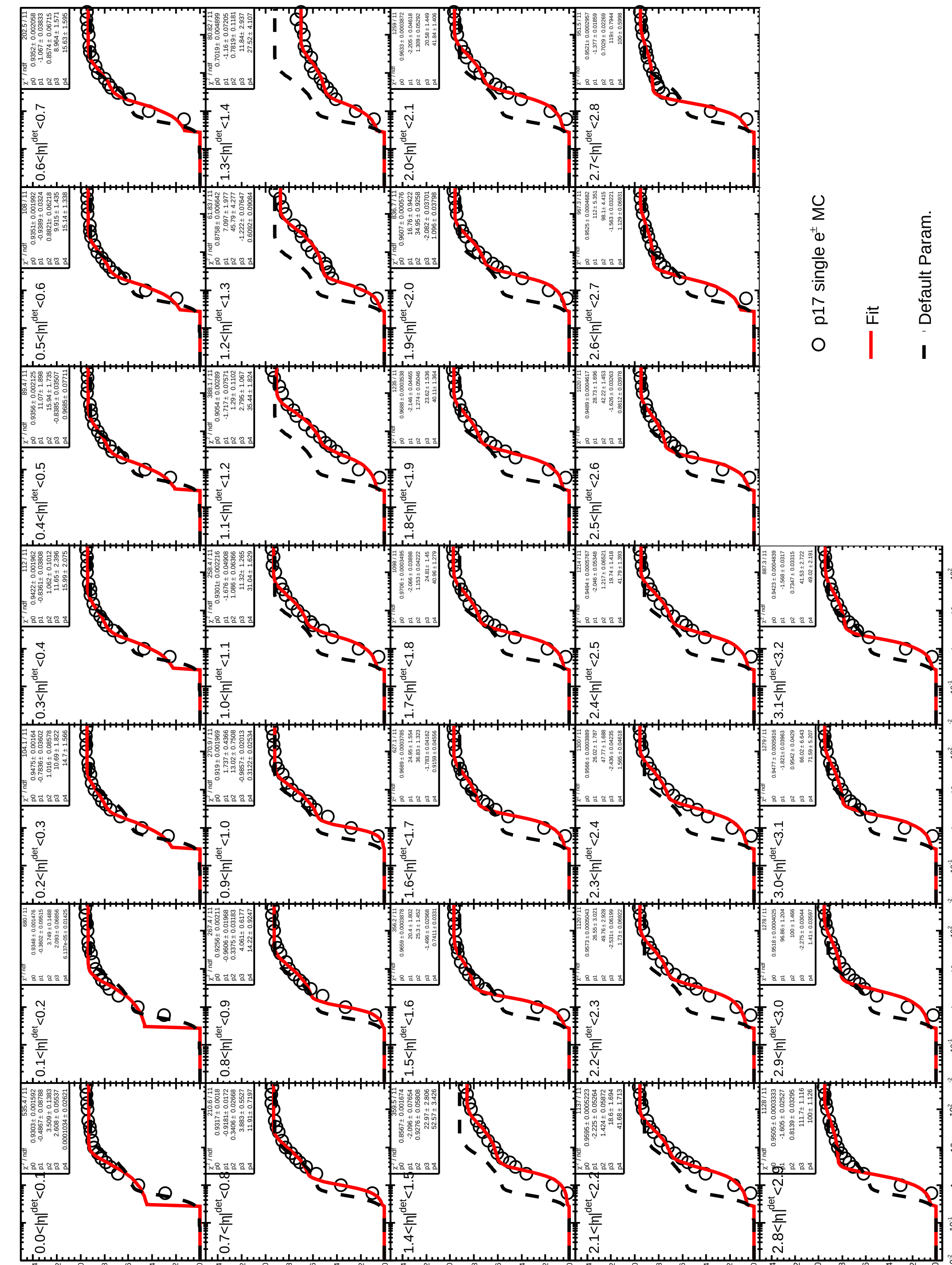

Figure 38: MC single electron response from p17 single $e^{\pm}$ MC sample, produced with ZS turned on. The black dashed line corresponds to the single electron response from Run IIA W mass studies. The red line is a fit to the MC points in black circles.

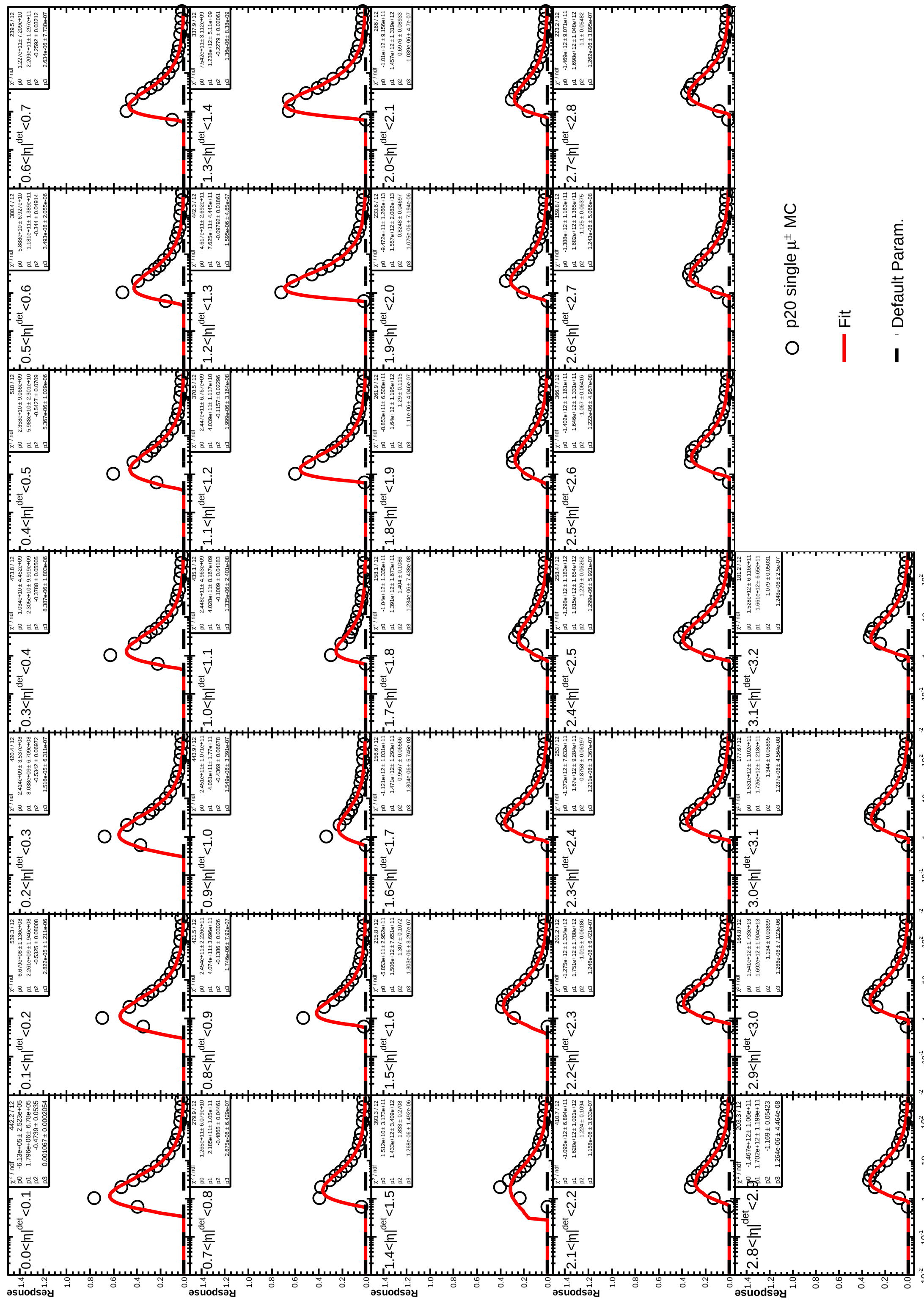

Figure 39: MC single electron response from p17 single $\mu^{\pm}$ MC sample, produced with ZS turned on. The black dashed line corresponds to 0. The red line is a fit to the MC points in black circles.

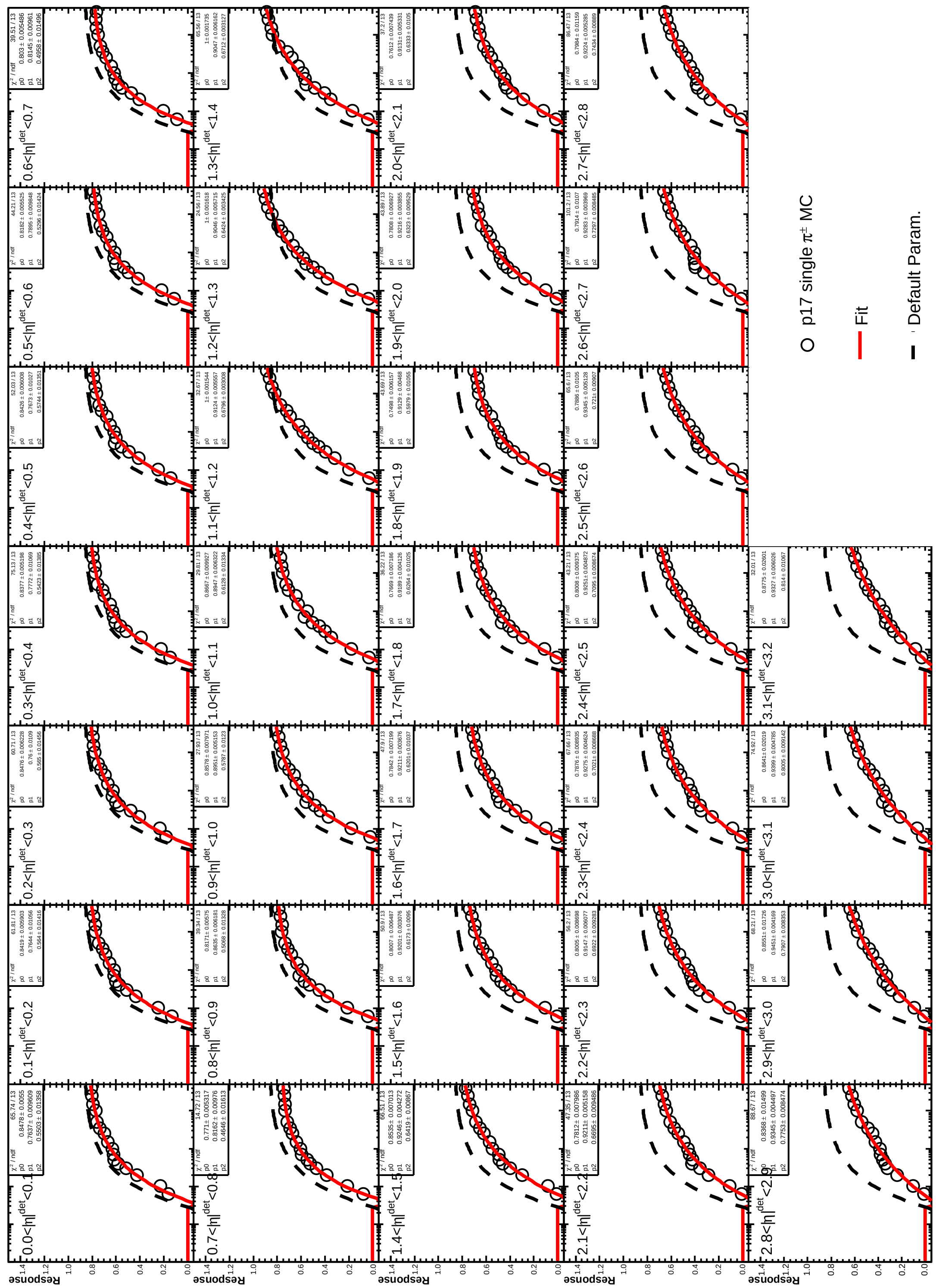

Figure 40: MC single pion response from p17 single $\pi^{\pm}$ MC sample, produced with ZS turned on. The black dashed line corresponds to the single pion response from Run IIA JES studies. The red line is a fit to the MC points in black circles.

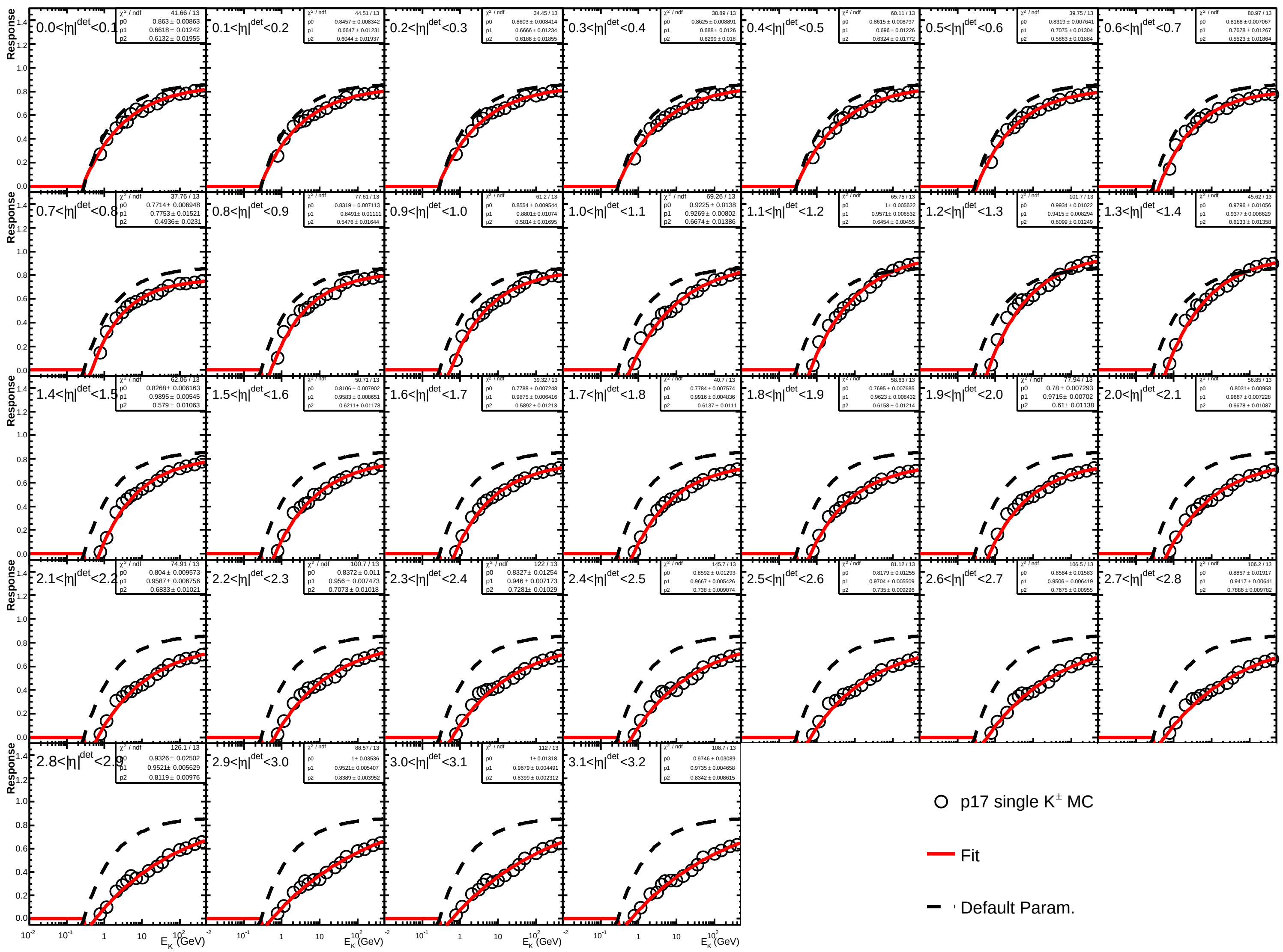

Figure 41: MC single kaon response from p17 single $K^{\pm}$ MC sample, produced with ZS turned on. The black dashed line corresponds to the single pion response from Run IIA JES studies. The red line is a fit to the MC points in black circles.

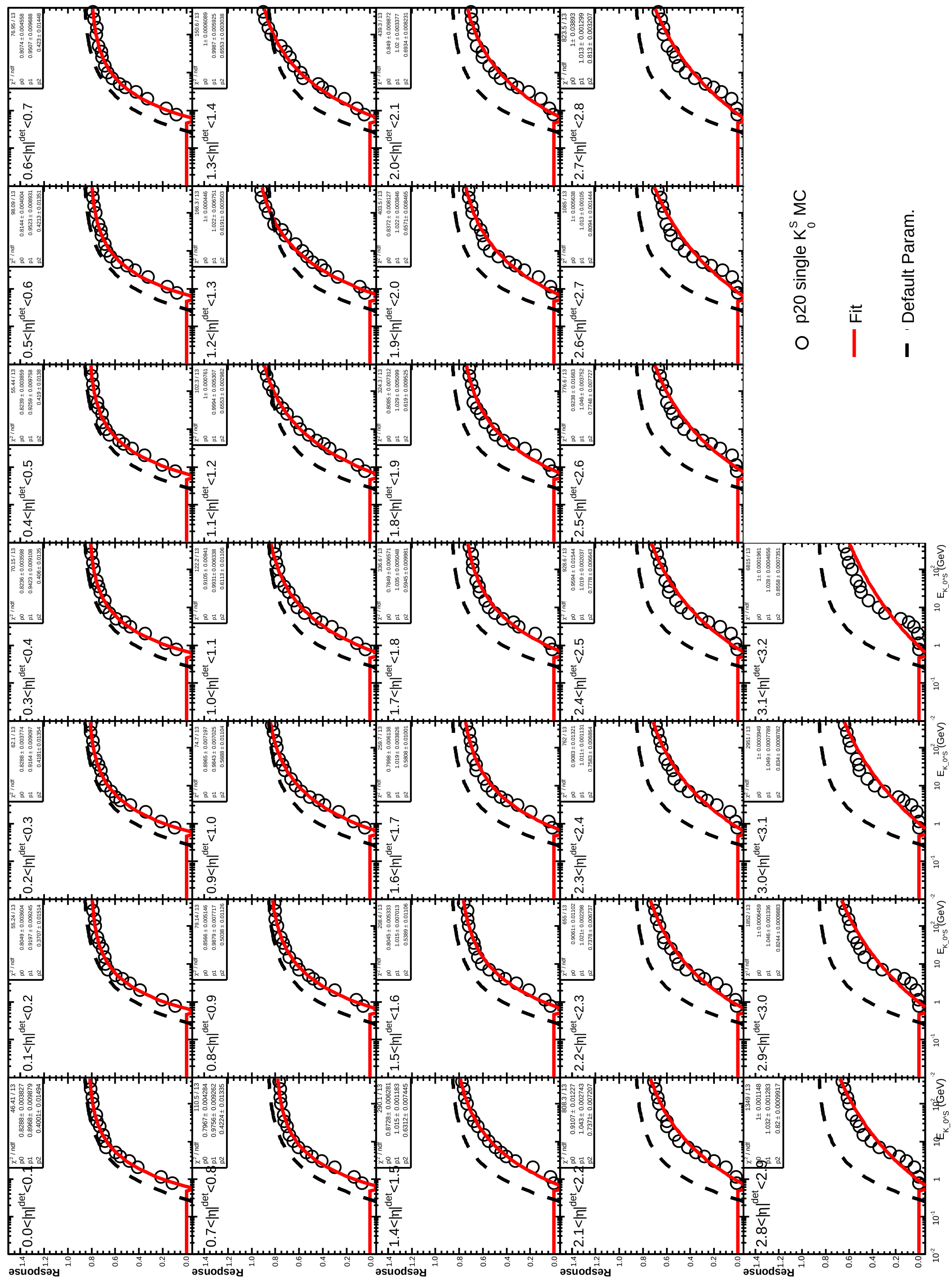

Figure 42: MC single kaon response from p17 single K_0^S MC sample, produced with ZS turned on. The black dashed line corresponds to the single pion response from Run IIA JES studies. The red line is a fit to the MC points in black circles.

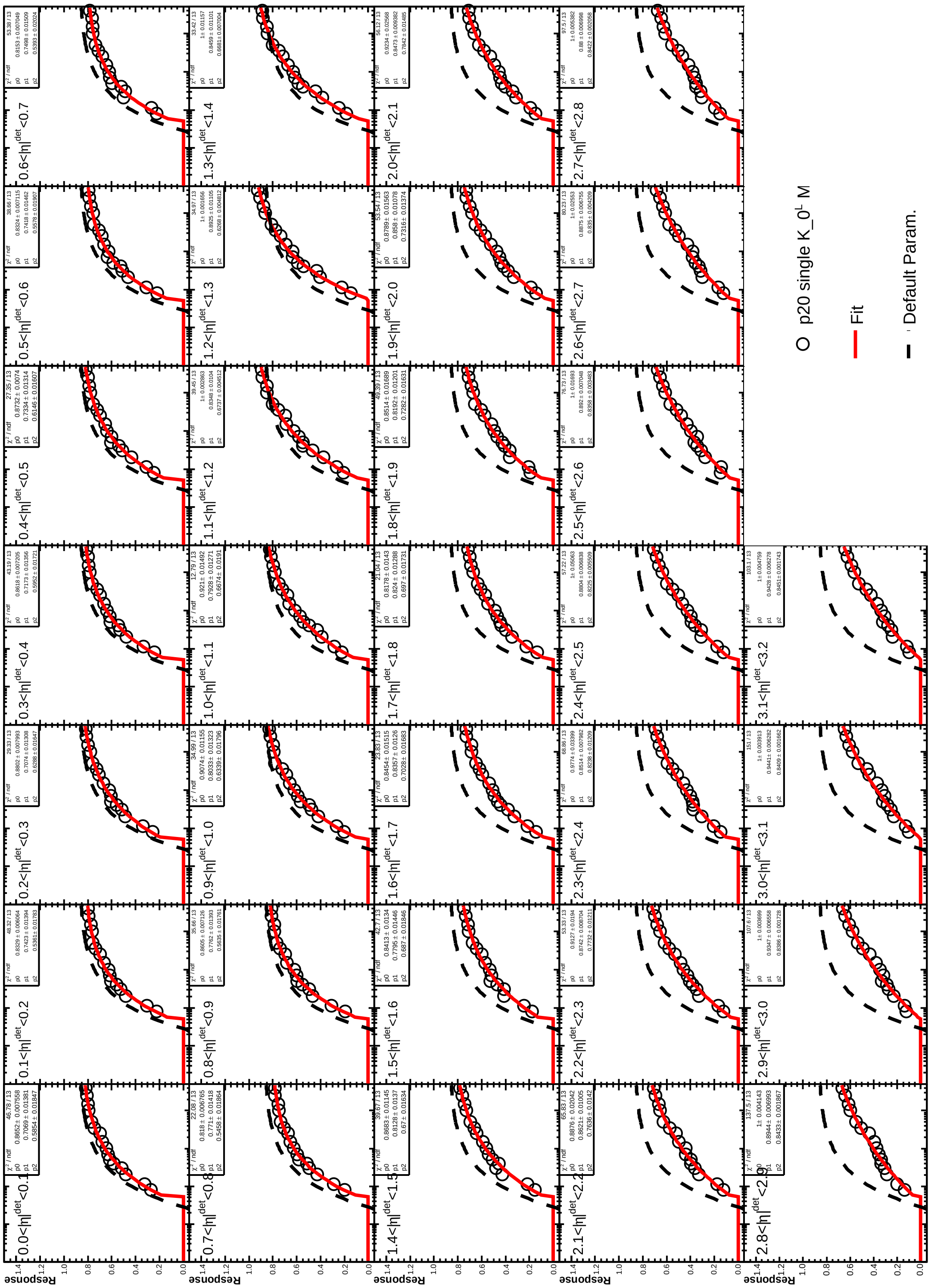

Figure 43: MC single kaon response from p17 single K_0^L MC sample, produced with ZS turned on. The black dashed line corresponds to the single pion response from Run IIA JES studies. The red line is a fit to the MC points in black circles.

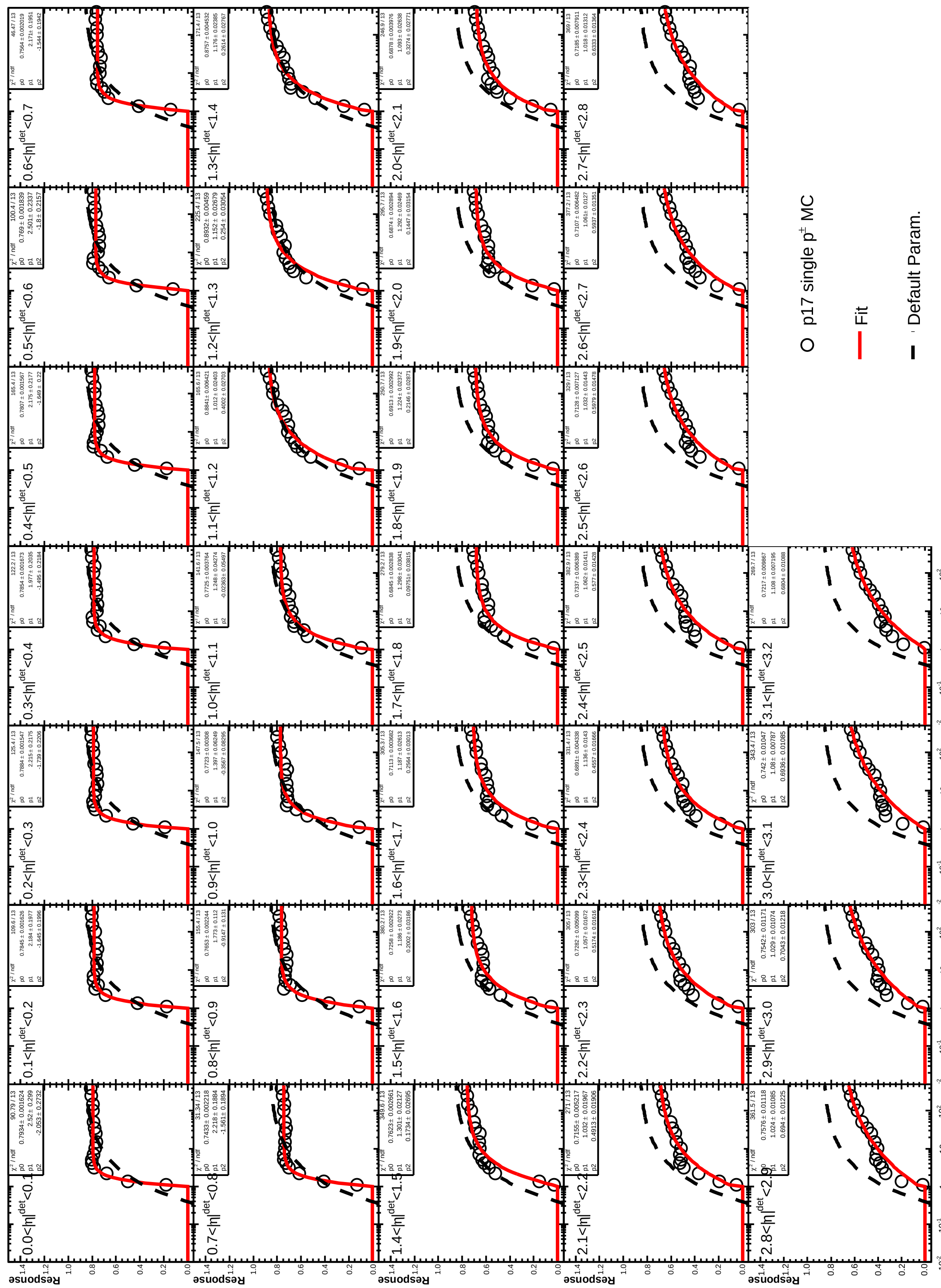

Figure 44: MC single proton response from p17 single $p^{\pm}$ MC sample, produced with ZS turned on. The black dashed line corresponds to the single proton response from Run IIA JES studies. The red line is a fit to the MC points in black circles.

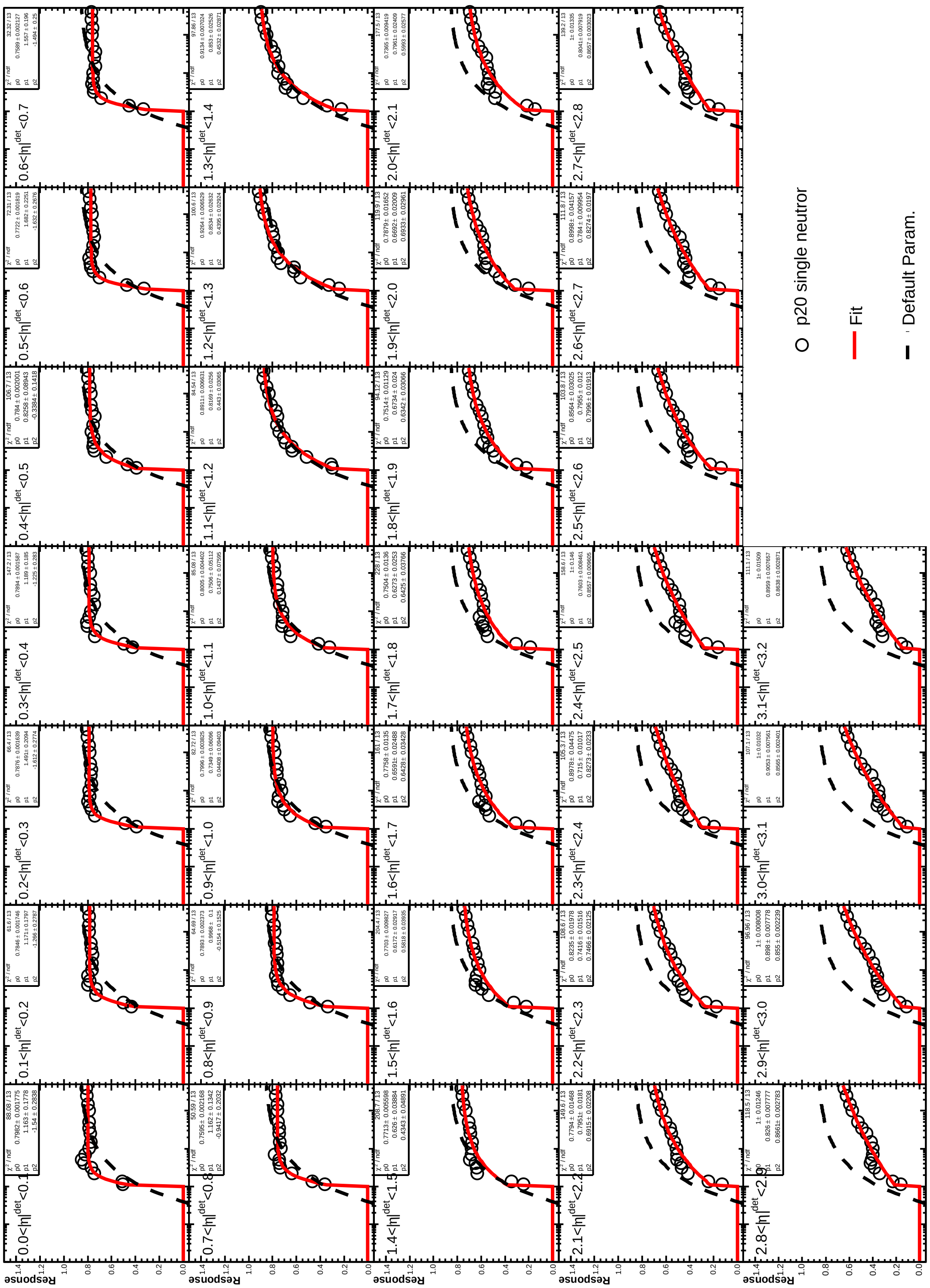

Figure 45: MC single proton response from p17 single n MC sample, produced with ZS turned on. The black dashed line corresponds to the single proton response from Run IIA JES studies. The red line is a fit to the MC points in black circles.

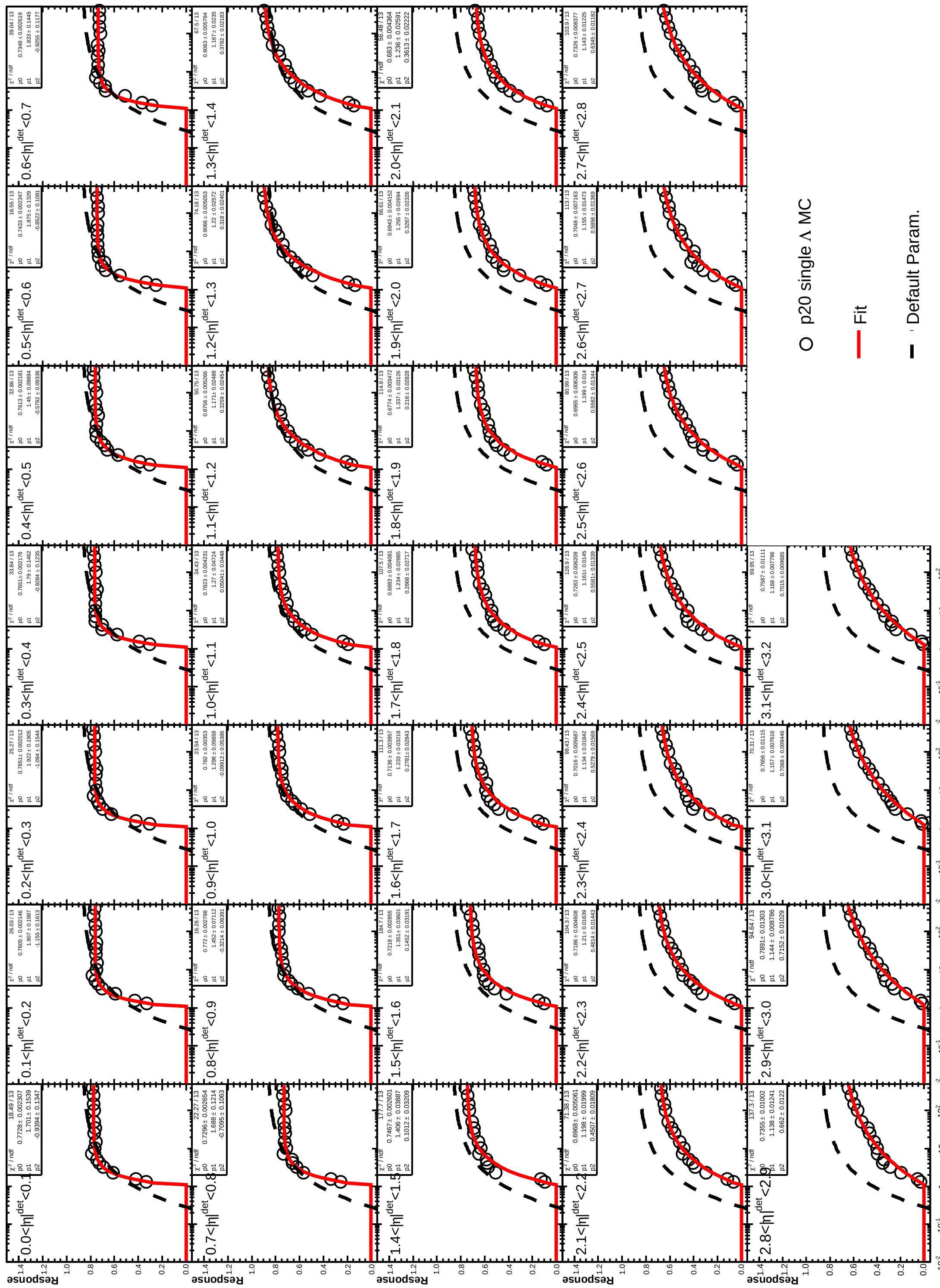

Figure 46: MC single proton response from p17 single Λ MC sample, produced with ZS turned on. The black dashed line corresponds to the single pion response from Run IIA JES studies. The red line is a fit to the MC points in black circles.

D MC Closure Test on γ+jet MC Samples Using MC Single Particle Responses With Zero Suppression Turned On

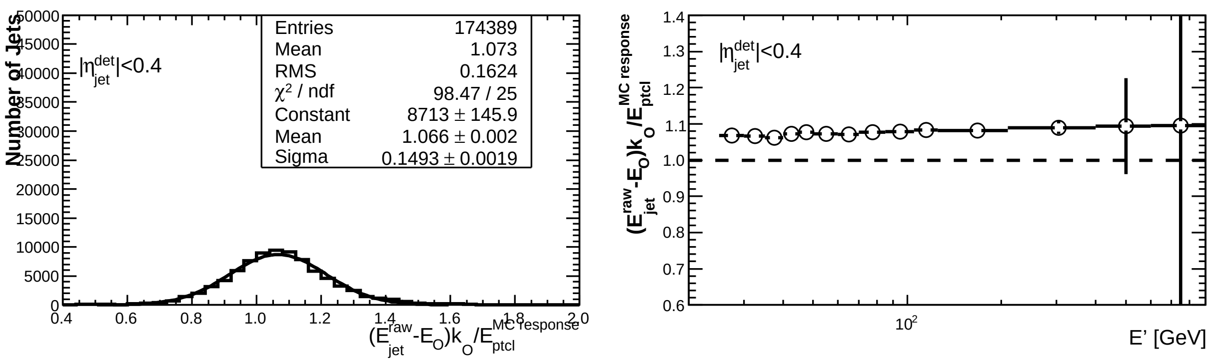

Figure 47: MC closure test for jets in p17 γ+jet MC sample for $|\eta^{jet}_{det}| < 0.4$. The single particle MC responses are derived with ZS turned on. The x-axis E' is given by $p^{\gamma}_{T} \cdot cosh(\eta^{jet})$.

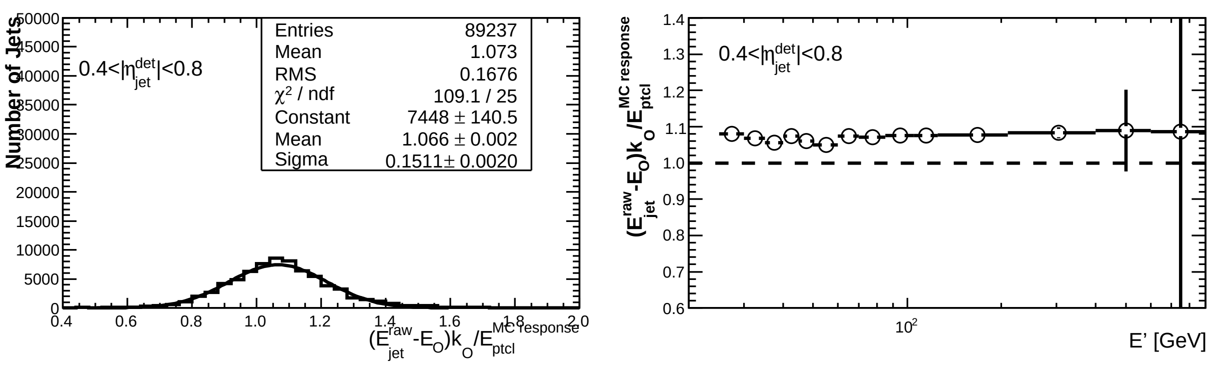

Figure 48: MC closure test for jets in p17 γ+jet MC sample for $0.4 < |\eta^{jet}_{det}| < 0.8$. The single particle MC responses are derived with ZS turned on. The x-axis E' is given by $p^{\gamma}_{T} \cdot cosh(\eta^{jet})$.

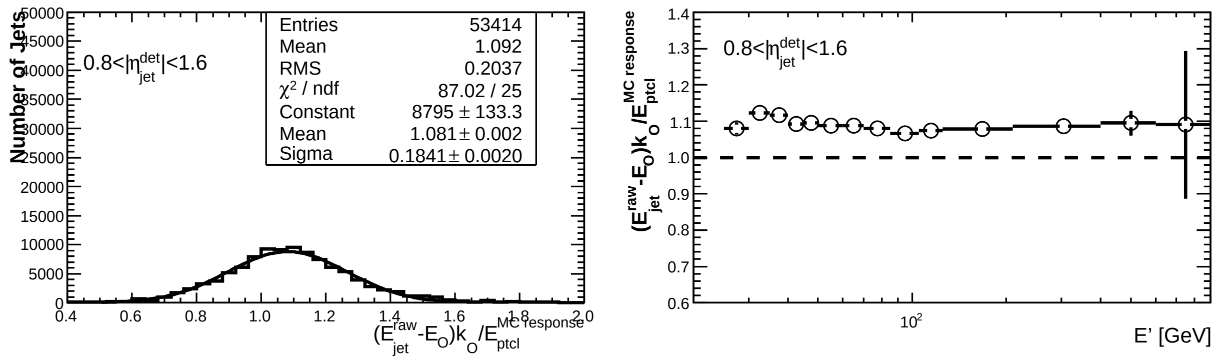

Figure 49: MC closure test for jets in p17 γ+jet MC sample for $0.8 < |\eta_{det}^{jet}| < 1.6$. The single particle MC responses are derived with ZS turned on. The x-axis E' is given by $p_T^{\gamma} \cdot cosh(\eta^{jet})$.

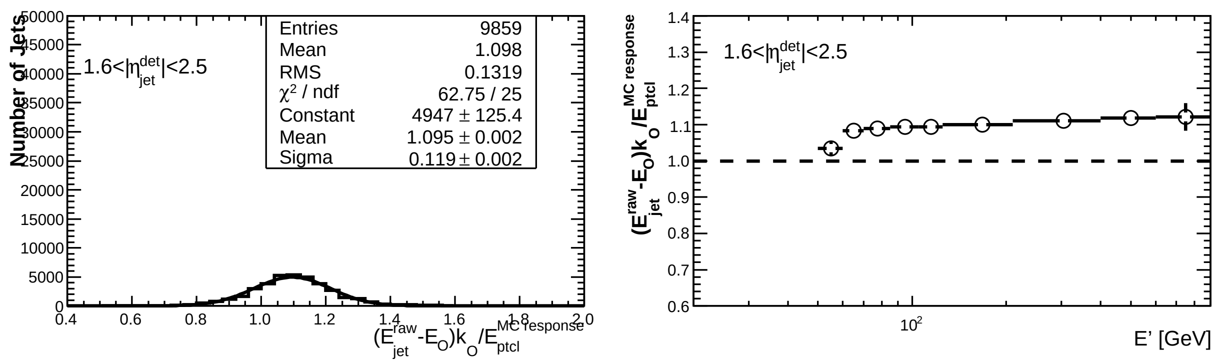

Figure 50: MC closure test for jets in p17 γ+jet MC sample for $1.6 < |\eta_{det}^{jet}| < 2.5$. The single particle MC responses are derived with ZS turned on. The x-axis E' is given by $p_T^{\gamma} \cdot cosh(\eta^{jet})$.

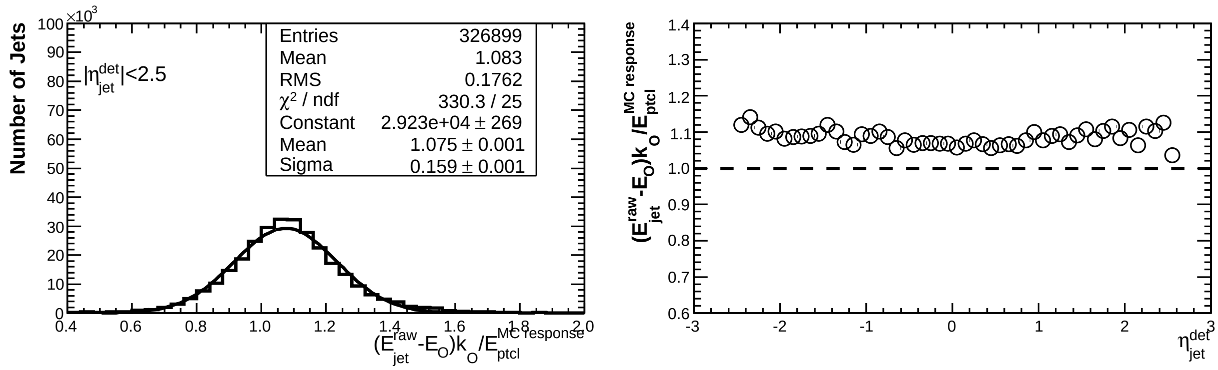

Figure 51: MC closure test for jets in p17 γ+jet MC sample for $|\eta_{det}^{jet}| < 2.5$. The single particle MC responses are derived with ZS turned on. The x-axis E' is given by $p_T^{\gamma} \cdot cosh(\eta^{jet})$.